SEISMIC RESPONSE AND POST-LIQUEFACTION ANALYSIS OF THE 1990 DASHIHE TAILINGS DAM

by

Carlos V. Amante

B.Sc., The University of the Philippines, 1984
M.Eng., Kanazawa University (Japan), 1991

A THESIS SUBMITTED IN PARTIAL FULFILLMENT OF

THE REQUIREMENTS FOR THE DEGREE OF

MASTER OF APPLIED SCIENCE

in

THE FACULTY OF GRADUATE STUDIES

(Department of Civil Engineering)

We accept this thesis as conforming
to the required standard

THE UNIVERSITY OF BRITISH COLUMBIA

August 1993

In presenting this thesis in partial fulfillment of the requirements for an advanced degree at the University of British Columbia, I agree that the Library shall make it freely available for reference and study. I further agree that permission for extensive copying of this thesis for scholarly purposes may be granted by the head of my department or by his or her representatives. It is understood that copying or publication of this thesis for financial gain shall not be allowed without my written permission.

Department of Civil Engineering
The University of British Columbia
2324 Main Mall
Vancouver, B.C., Canada
V6T 1Z4

Date: Sept. 15, 1993

ABSTRACT

This thesis presents a preliminary research study of the seismic safety of the Dashihe Tailings Dam in its 1990 condition using state-of-the-art analytical and empirical procedures. The study involves an analysis of the seismic response and post-liquefaction behavior of the dam using the 1976 Tangshan and Luanxian earthquake records as input. The seismic response of the dam was analyzed using the TARA-3 program (Finn et al., 1986). Zones of liquefaction are predicted to develop under the pond and the beach. Extensive cracking is expected to occur in a significant portion of the beach. A post-liquefaction flow deformation analysis of the dam was also performed using the program TARA-3FL (Finn and Yogendrakumar, 1989). The analysis shows that most of the deformations would occur by sliding of materials under the pond and in the area of the beach near the pond margin. Despite these deformations, the dam is expected to remain operational after the earthquake.

TABLE OF CONTENTS

LIST OF TABLES

Page No.

LIST OF FIGURES

Page No.

ACKNOWLEDGEMENT

I wish to express my sincere and deep gratitude to Professor W.D. Liam Finn of the Dept. of Civil Engineering for his valuable guidance and encouragement as well as financial support towards the completion of this research work.

I would also like to thank my wife and children for constantly providing me inspiration and support during my study.

I also appreciate the valuable assistance given by Mr. Guoxi Wu of the Dept. of Civil Engineering and Mr. Hongbo Xin of CRIBC (Beijing, China).

Carlos V. Amante

Chapter 1

INTRODUCTION

The Dashihe Tailings Dam is a typical upstream tailings impoundment structure located about 50 km northeast of Tangshan City in North China. The dam, operated by Capital Iron and Steel Company, was first constructed in 1961 and is being raised at a rate of about 2 m per year. The dam was originally designed to reach a height of 45 m with a storage capacity of 36.5 million cubic meters. To meet increased mine production in 1988, the design height was increased to 64 m with a storage capacity of 61 million cubic meters. However, the total height of the dam had reached 70 m in 1990. The possibility of raising the dam substantially higher is now being considered in order to prolong the service life of the tailings pond.

On July 28, 1976, the dam was shaken by the main shock of the Tangshan Earthquake (M = 7.8) with an epicentral distance of 43 km, and 16 hours later by another major shock (M = 7.1) at Luanxian with an epicentral distance of 19 km. These seismic events were estimated to cause accelerations of the order of 0.12 g and 0.18 g, respectively, in bedrock at the dam site. The 1976 earthquakes caused minor cracking on the downstream shell of the dam. Widespread evidence of liquefaction were observed on the beach area, with large cracks, sand boils and some evidence of sliding of materials into the pond. However, the dam remained operational without any need for repairs.

Since the Dashihe Tailings Dam is situated in an active seismic region, a major factor requiring consideration in planning any further raising of the dam is an estimation of its

performance during the design earthquake. Cooperative studies by Canadian and Chinese researchers have been conducted to assess the present condition of the dam by careful site investigations (Gao et al., 1991) and complementary laboratory studies (Li et al., 1992) using the state-of-the-art techniques. The research groups also attempted to simulate the important aspects of the seismic response of the dam during the 1976 earthquakes using various methods. Finn and Xin (1992) successfully simulated the seismic response and triggering of liquefaction of the dam during the 1976 earthquake using the nonlinear effective stress analysis program TARA-3 (Finn et al., 1986). They also analyzed the post-liquefaction behavior of the 1976 dam using the program TARA-3FL (Finn and Yogendrakumar, 1989). The results of their studies provided some validation for using their procedures for assessing the seismic capacity of the dam in its planned configuration.

A preliminary study of the seismic safety of the Dashihe Tailings Dam in its 1990 condition is presented in this thesis. The study involves an analysis of the seismic response and post-liquefaction behavior of the dam using the 1976 Tangshan and Luanxian earthquake records as input. Chapter 2 gives a description of the Dashihe Tailings Dam - the site conditions, construction history and seepage control. Chapter 3 presents the description of the 1976 Tangshan Earthquake, the probable ground motions, and the observed seismic performance of the dam during the earthquake. Chapter 4 describes the results of field investigations performed in 1990 to derive the required soil parameters for the study. Chapter 5 presents the results and discussions of the dynamic analysis performed using the TARA-3 program. Chapter 6 describes the results of post-liquefaction analysis of the dam. The summary and conclusions derived from the study are given in Chapter 7.

Chapter 2

DESCRIPTION OF DASHIHE TAILINGS DAM

2.1 Site Conditions

The Dashihe Iron Mine, operated by Capital Iron and Steel Company, is located about 50 km northeast of Tangshan City in Qianan County, Hebei Province in North China. The Dashihe tailings impoundment (Fig. 2.1) lies across the Mengjiachong Valley, 4 km northwest of the concentration plant. Surrounded with mountains in three sides, the Mengjiachong Valley is 1.8 km long from north to south and has a drainage area of 2.8 km^2. The main dam (#1 dam) stands at the valley mouth in the north. As the main dam increased in height, #2, #3, and #4 auxiliary dams were subsequently built and linked up with the main dam so that the total length of the dam had now reached 800 meters. Two other auxiliary dams (#5 and #6) were constructed in the southern end of the valley in order to retain the water in the pond.

2.2 Construction History

The construction of the Dashihe Tailings Dam is being performed using the upstream embankment raising method (Vick, 1983), illustrated in Fig. 2.2. A starter dike is first constructed and tailings are deposited peripherally from its crest to form a beach and pool. This beach then becomes the foundation for a second perimeter dike or sub-dike. The construction is done using bulldozers. The embankment height is raised about 2 meters per year. Each sub-dike is about 2 meters high, 10 meters wide at the bottom and 7 meters

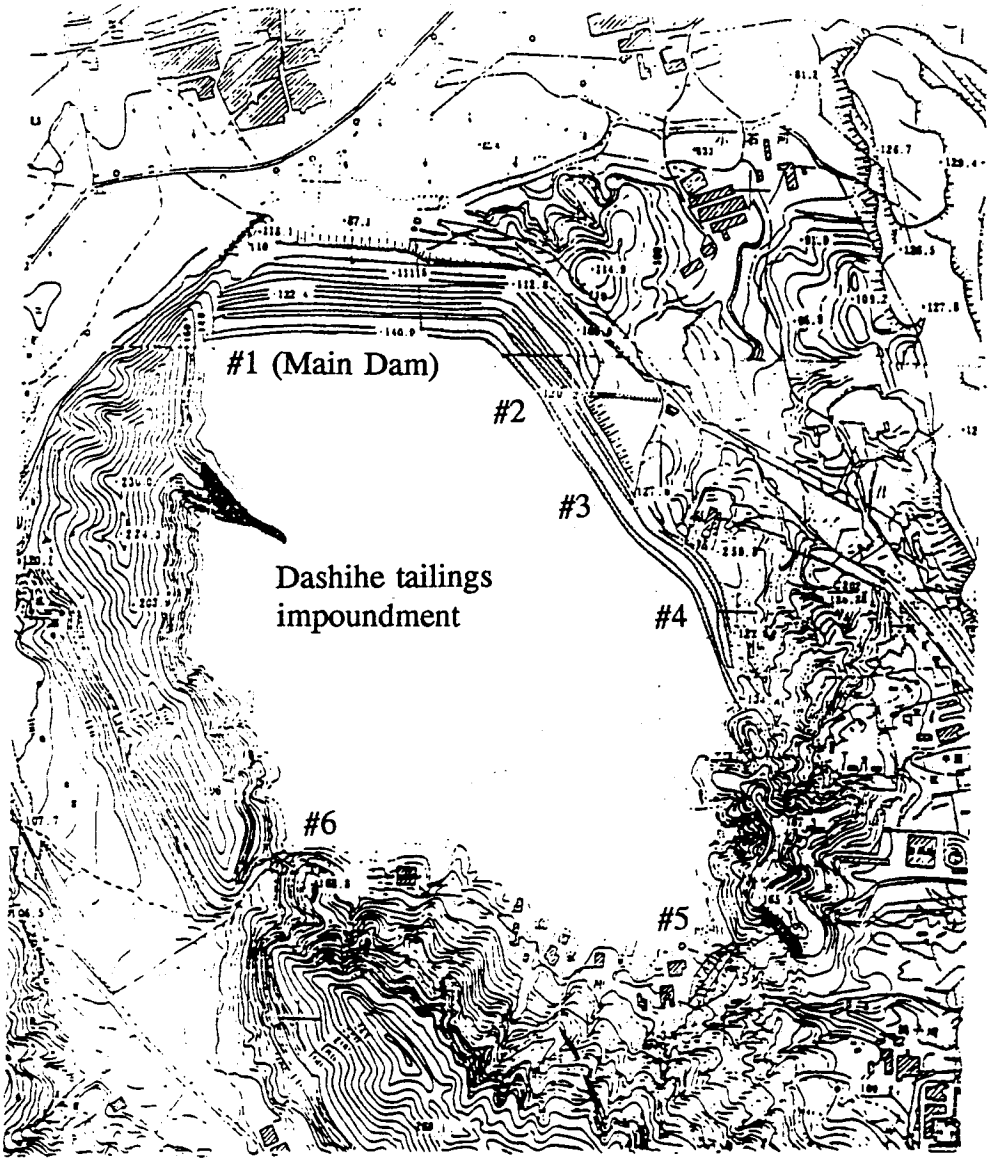

Fig. 2.1 - Plan view of the Dashihe Tailings Impoundment
(After CRIBC, 1989)

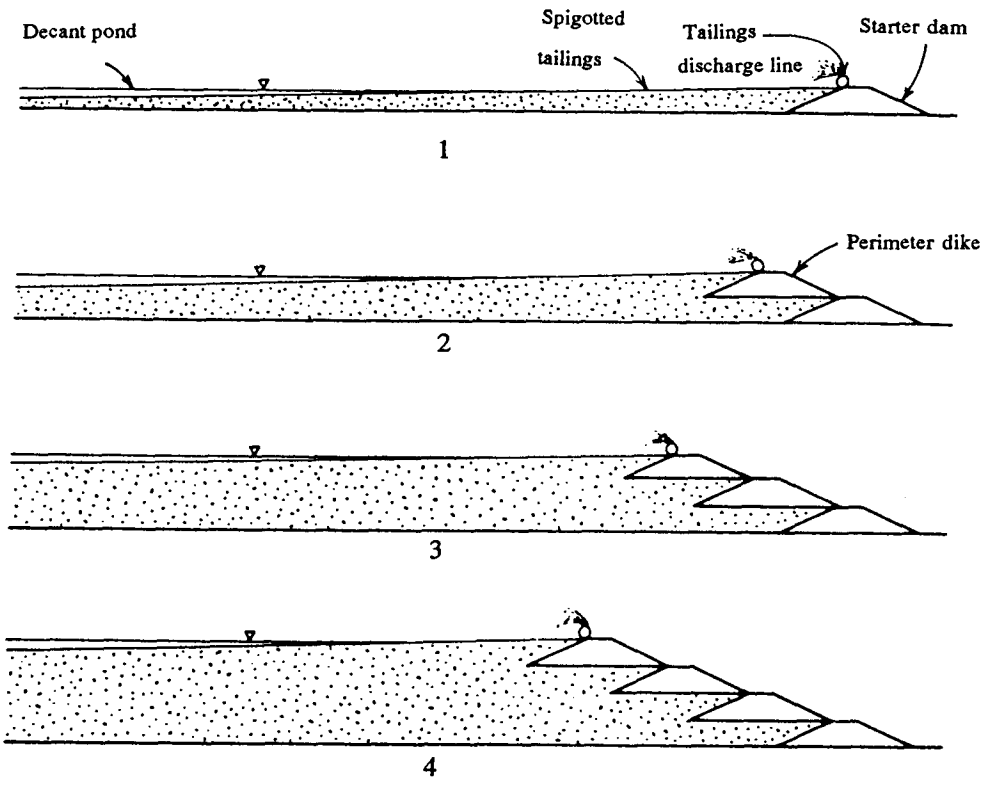

Fig. 2.2 - Sequential upstream construction of a tailings dam
(After Vick, 1983)

wide at the crest. The average external slope is 1:5. The starter dike was constructed of loam, placed in layers and rolled. The dike is about 14 meters high and 338 meters long. The foundation materials consist of about 10 meters of interbedded loam and cobble strata overlying bedrock.

Tailings deposition began in 1962. By 1976, the dam had reached a height of 37 meters, and by 1990 the total dam height was 70 meters (Fig. 2.3). The dam profile (Fig. 2.3) is highly stratified with the coarse-grained materials deposited near the crests of the sub-dikes where the tailings are discharged. The fine-grained materials are deposited near the pond. This pattern of deposition is characteristic of the upstream construction method. Because of the stratified nature and the variable particle composition of each layer, the Dashihe tailings materials are classified into six soil types, namely, medium sand, fine sand, silty sand, sandy loam, loam and clay.

2.3 Seepage Control

During the early stage of construction of the dam in 1965, a very high phreatic surface caused the seepage water to break-out on the downstream shell near the crest of the starter dam. In 1969, horizontal internal drains had been installed on the inner slope of the starter dam. By 1976, these drains were not operating properly due to excessive siltation leading to a major slide of the materials in the downstream slope between the crest of the starter dam and the second sub-dike. The internal drains were replaced by an outer drainage ditch and a number of relief wells were installed. These measures caused the phreatic surface to drop by 12 meters just before the July (1976) earthquake. However, by 1980, the drainage

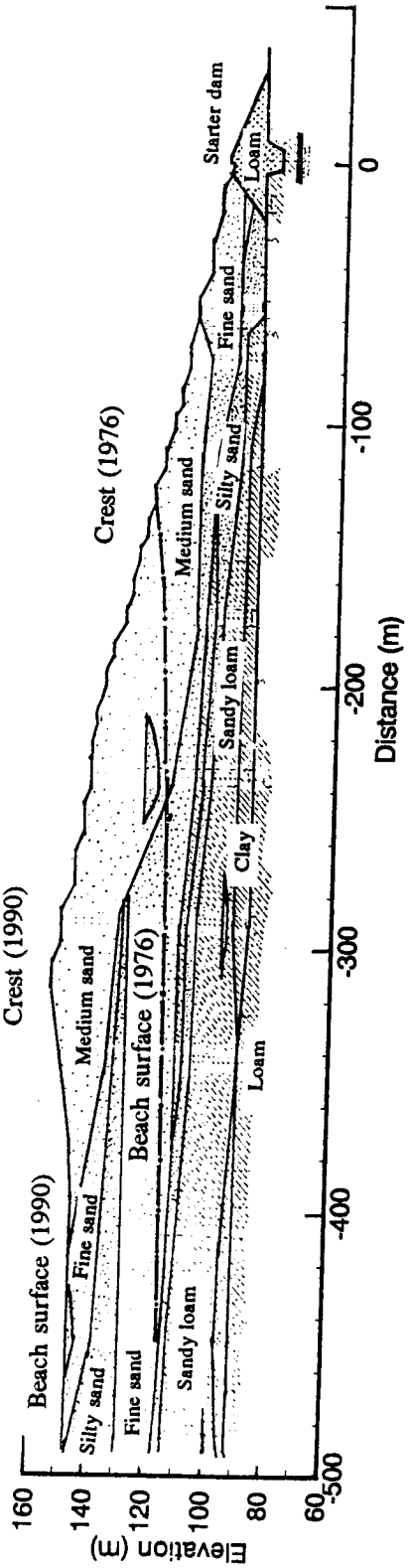

Fig. 2.3 - Dashihe Tailings Dam profile in 1976 and 1990 (Main dam cross-section)

measures ceased to be effective again and the phreatic surface reached the crest of the starter dam where it still remained in 1990. This increase in the level of the phreatic surface increases the potential for liquefaction and large deformations.

Chapter 3

THE 1976 TANGSHAN EARTHQUAKE

3.1 Earthquake Description

A destructive earthquake of magnitude M = 7.8 struck Tangshan City, Hebei Province at 3:43 a.m. (local time) on July 28, 1976. The effects of the earthquake were felt over an area of approximately 85,000 km^2. The epicentre was located in the southern part of the city at 127.8°E and 40.7°N, about 43 km away from the Dashihe Dam site. The intensity in the epicentral area was estimated at 11 on the Modified Mercalli Intensity (MMI) scale, and the intensity at the Dashihe Dam site was estimated to be between 7 and 8 on MMI scale (Fig. 3.1). Another strong earthquake with magnitude M = 7.1 also occurred about 16 hours later at Lwnxian, 118.5°E and 39.7°N, about 19 km from the Dashihe Dam site. Its intensity of shaking in epicentral area was reported to be 9 on MMI scale.

3.2 Estimated Ground Motions at the Dashihe Dam Site

The peak ground accelerations at the site of the Dashihe Tailings Dam due to the 1976 seismic events were estimated using an attenuation relationship proposed by Hu et al. (1980),

$$\ln A_m = 1.078 + 0.567\,M - 1.881 \ln (R + 10) \qquad (3.1)$$

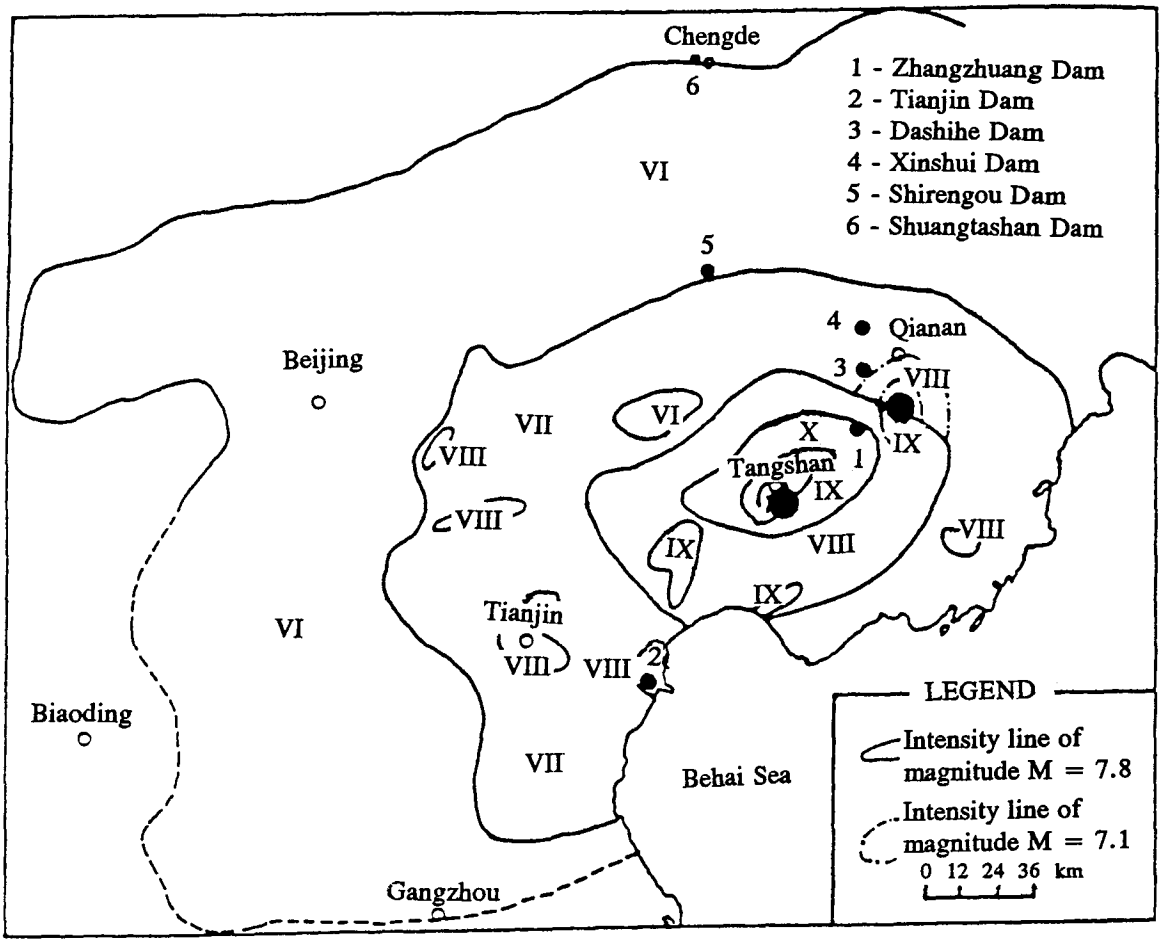

Fig. 3.1 - Intensity map during the 1976 Tangshan and Luanxian earthquakes (After CRIBC, 1989)

in which A_m is the maximum acceleration in units of g, the acceleration due to gravity; M is the earthquake magnitude, and R is the hypocentral distance in km. This relationship is based on intensity attenuation laws for the 1976 Tangshan earthquake and the results of attenuation research from western North America. This attenuation law indicates a peak acceleration in bedrock at the dam site of the order of 0.12 g due to the main shock of the Tangshan earthquake, and 0.18 g due to the later earthquake at Luanxian.

The ground motions selected for the study of the performance of Dashihe Dam during the 1976 earthquake were developed by a research team from the Central Research Institute of Building and Construction (CRIBC), Ministry of the Metallurgical Industry in Beijing (CRIBC, 1989). These motions, scaled to peak accelerations of 0.12 g and 0.18 g and duration of 20 seconds, are shown in Fig. 3.2. The Luanxian record has many pulses with high frequency content compared with the Tangshan record, which is characteristic of near-field earthquake motions. The peak ordinate of the Luanxian earthquake is 50 % more than that of the Tangshan earthquake. However, there is only one pulse that contains the peak value of 0.18 g. The rest of the record has many ordinates substantially below 0.1 g.

The response spectra of the acceleration records of both the Tangshan and Luanxian earthquakes were computed for linear-elastic single-degree-of-freedom systems with 5 % and 10 % viscous damping ratios. The results, presented in Fig. 3.3, indicate that the Luanxian earthquake generates greater response for systems with periods shorter than 0.3 seconds. Systems with periods longer than 0.3 seconds, however, respond more to the Tangshan earthquake shaking.

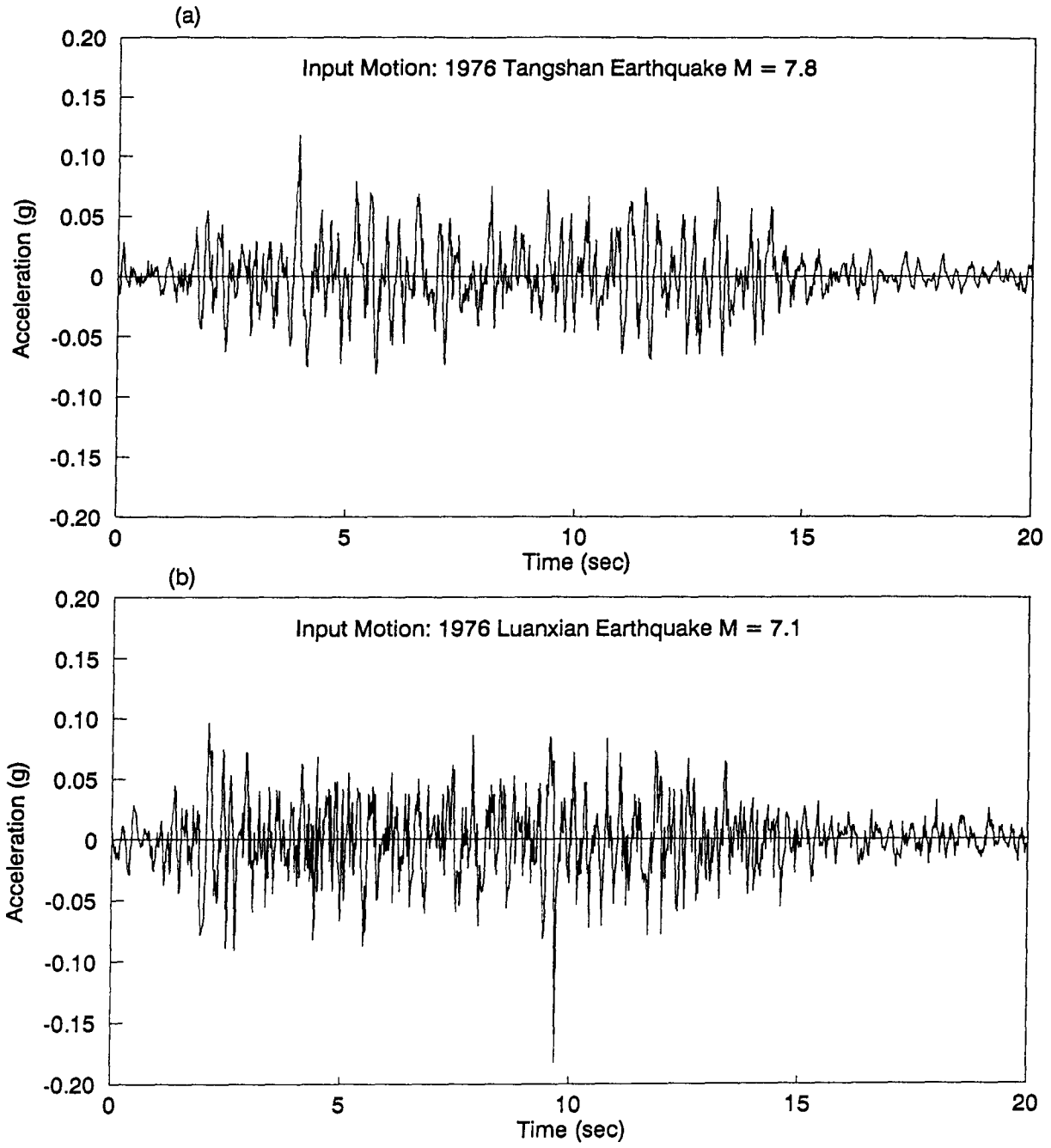

Fig. 3.2 - Estimated ground motions at Dashihe Dam site for the Tangshan and Luanxian earthquakes in 1976

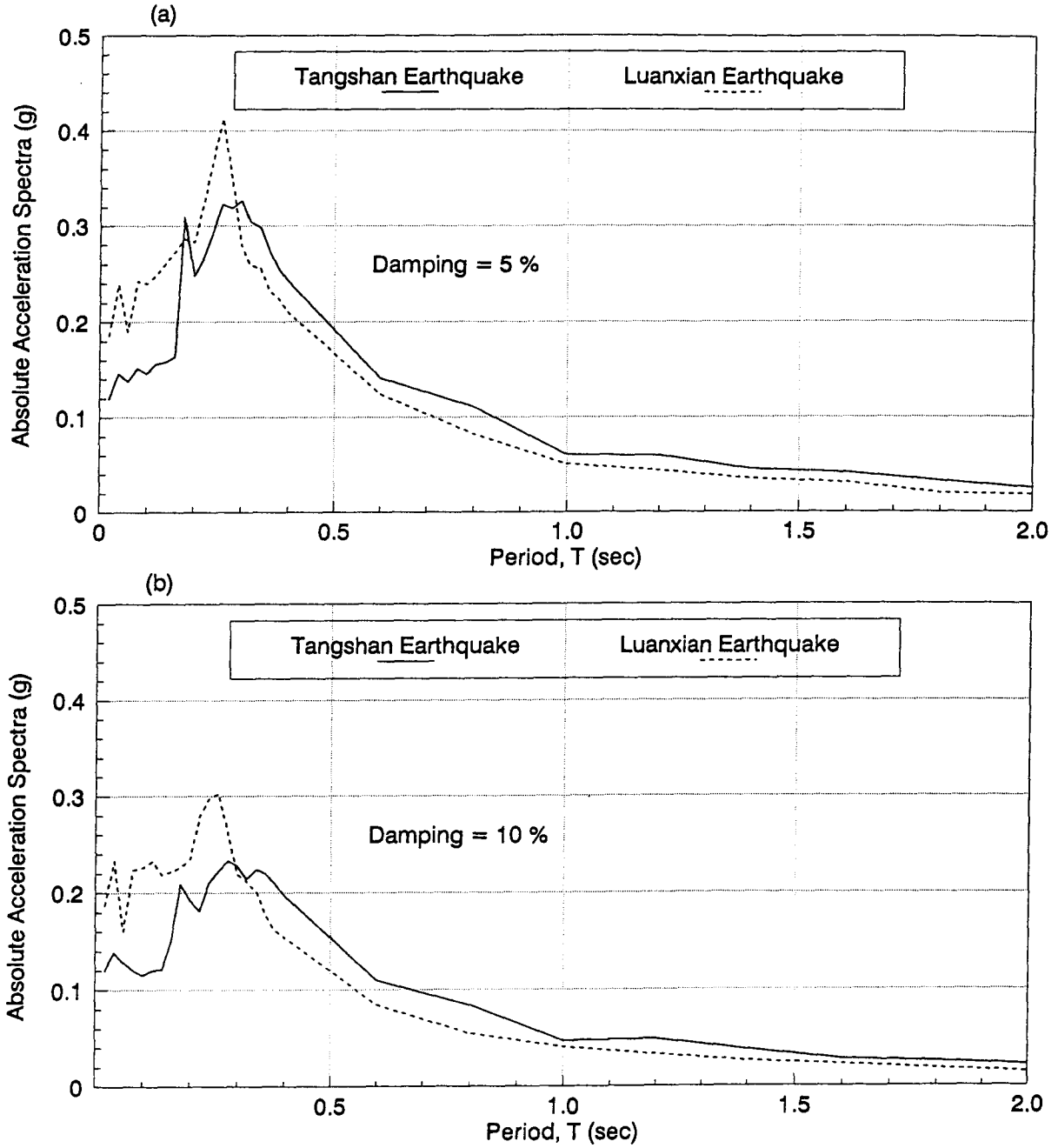

Fig. 3.3 - Computed response spectra for the Tangshan and Luanxian earthquakes

3.3 Seismic Performance of Dashihe Dam in 1976

The 1976 Tangshan Earthquake was considered to be the most destructive earthquake of this century resulting in more than 242,000 deaths and 164,000 injuries. The earthquake caused serious damage to several important engineering facilities and public infrastructures such as buildings, bridges, roads and railway lines, buried structures, dams, etc.

The Dashihe Tailings Dam experienced varying degrees of structural damage as a result of the 1976 earthquake. However, the impoundment remained operational without any need for repairs. Minor cracking occurred on the downstream shell. At the fifth sub-dike, about 11 meters above the starter dam, a number of fissures developed parallel to the dam axis. The fissures were 20-30 mm wide and 10-20 meters long (Fig. 3.4). Many sandboils and water spouts were observed on the beach near the pond . The largest sandboil observed was 2 meters in diameter (Fig. 3.5). Fissures were also found parallel to the pond margin between the pond and about 80 meters from the crest (Fig. 3.6). The closer to the pond, the denser became the concentration of fissures. There were many tensile cracks, 20-700 mm wide, 10-30 meters in length, and up to 1 meter in depth. These fissures were parallel to each other. Elevation drop across the fissures reached a maximum of 0.5 meter (Fig. 3.6). From this, it is inferred that there was some significant sliding of surface materials in the beach towards the pond.

Fig. 3.4 - Earthquake-induced cracking in the downstream shell of Dashihe Dam observed during the 1976 earthquake (After CRIBC, 1989)

Fig. 3.5 - Sandboil observed in the beach of Dashihe Dam (1976)
(After CRIBC, 1989)

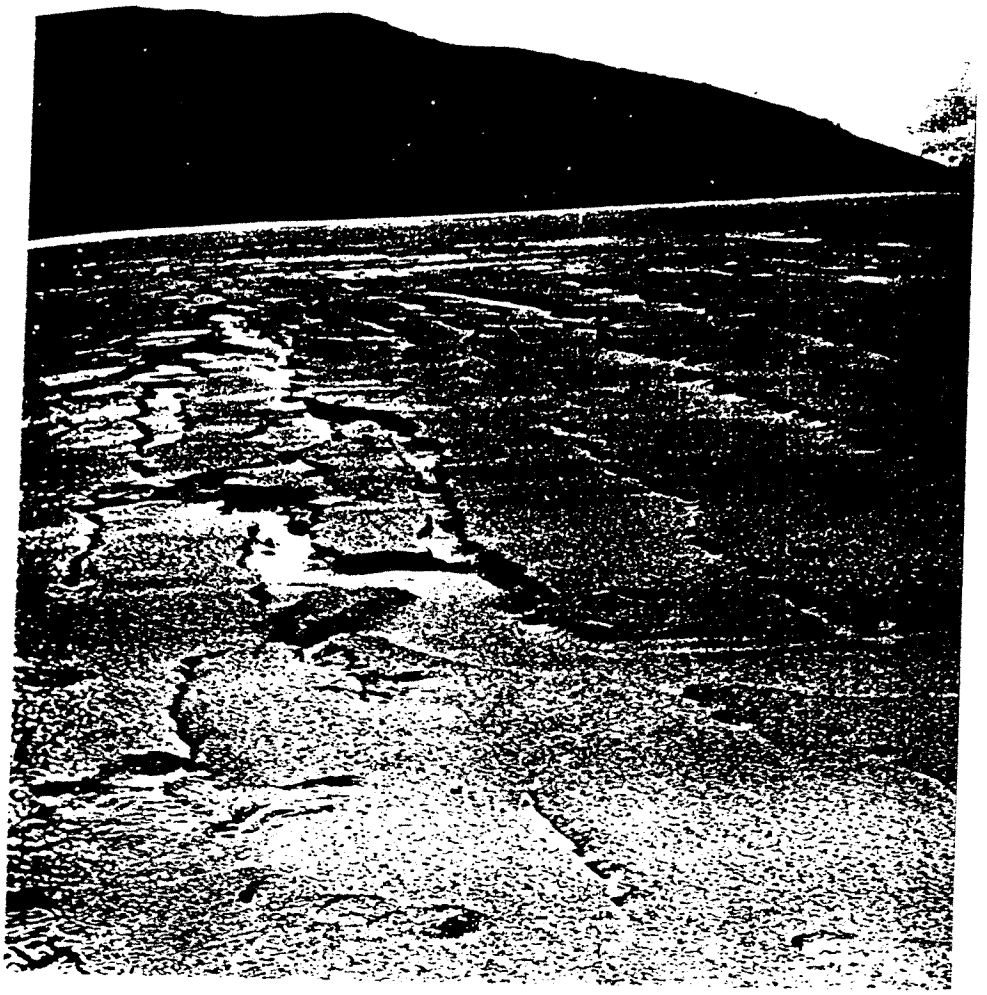

Fig. 3.6 - Earthquake-induced cracking in the beach of Dashihe Dam (1976) (After CRIBC, 1989)

Chapter 4

FIELD INVESTIGATIONS AND SOIL PROPERTIES

4.1 Distribution of $(N_1)_{60}$ in Dashihe Dam

Comprehensive field investigations were conducted in Dashihe Tailings Dam in 1980 and 1990. Details of the 1980 investigations were reported by CIGHS (1980) and the 1990 investigations by CRIBC (1990). The 1990 data were analyzed in detail by Gao et al. (1991) at the University of Alberta. This report provides the definitive database on the in-situ properties of the materials in the 1990 section of the dam. Laboratory investigations on samples retrieved from the 1990 site investigations were performed at CRIBC (1991) in Beijing. These data were subsequently analyzed by Li et al. (1992).

The site investigation in 1980 was based on the Standard Penetration Test (SPT) and some disturbed samples were retrieved. In 1990, both SPT and the Cone Penetration Test (CPT) were used to investigate the in-situ state and stratigraphy of the dam. In-situ densities were estimated using the nuclear logging wd undisturbed samples were retrieved and frozen for laboratory testing. In addition, seismic shear wave velocities were measured at selected locations.

SPT borings in 1990 were made along the three cross-sections shown in Fig. 4.1. The borings were made using an automatic trip hammer and followed a standard procedure in general accordance with the ASTM D1586-84.

The measured SPT blowcounts or N values have been normalized to an effective overburden pressure (σ_o) of 100 kPa or 1 tsf and to a driving energy ratio, ER, in the drill

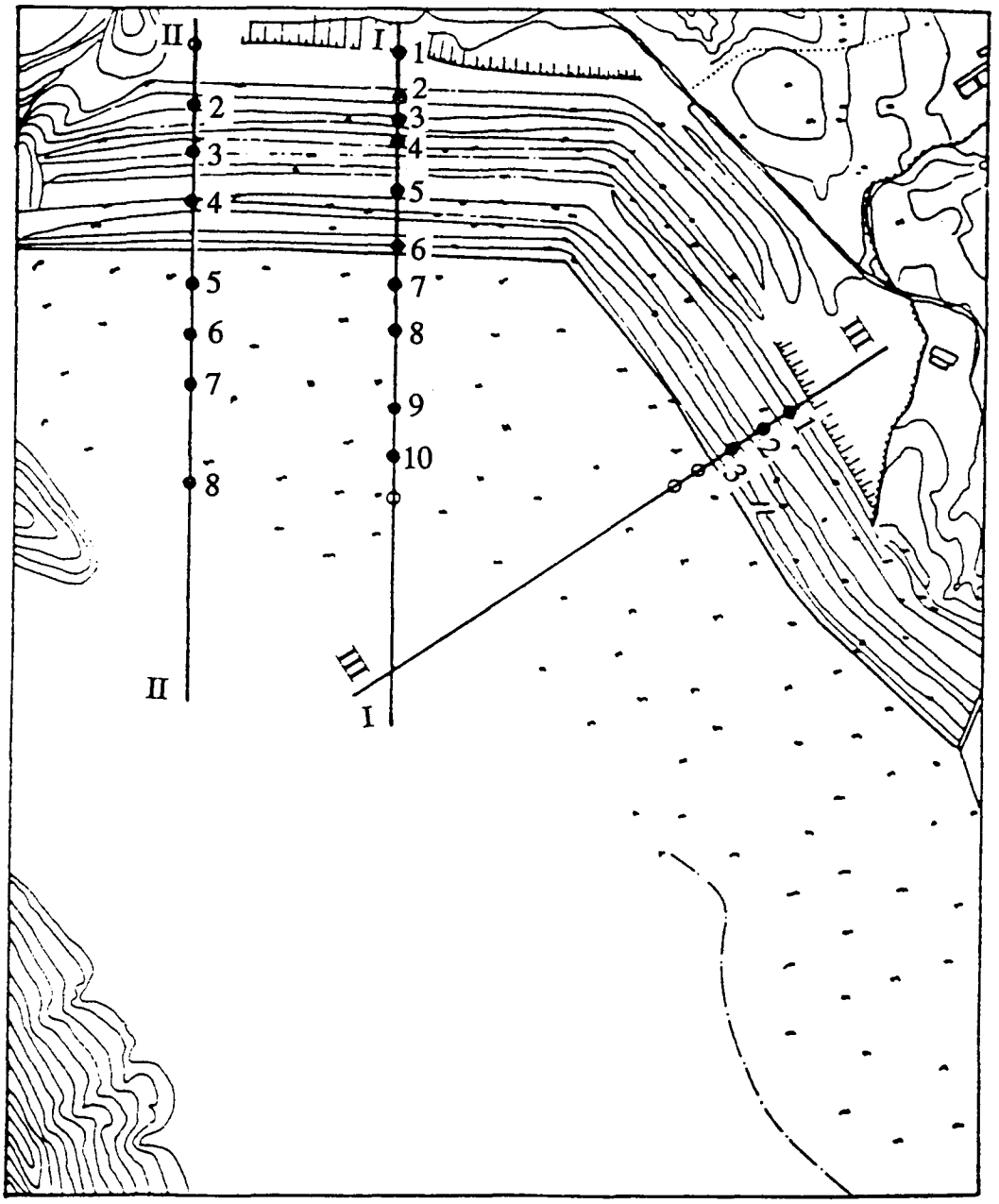

Fig. 4.1 - Dashihe Dam cross-sections for the field investigations in 1990 (After Gao et al., 1991)

rods of 60 % of the theoretical free-fall energy of the hammer, giving values designated $(N_1)_{60}$ and expressed as follows:

$$(N_1)_{60} = \left(\frac{P_a}{\sigma'_o}\right)^{1/2} \left(\frac{ER}{60}\right) N \qquad (4.1)$$

where P_a is the atmospheric pressure (100 kPa or 1 tsf) used as a reference stress. The formula for *ER* has been derived by Gao et al. (1991) based on SPT energy measurements performed in borehole I-4, as follows:

$$ER\ (\%) = 31 + 2.11\ z \leq 68\% \qquad (4.2)$$

where z is the soil depth in meters.

The distribution of $(N_1)_{60}$ based on the 1990 SPT soundings on cross-section I-I, the main section of Dashihe Dam used in seismic stability analysis, are summarized in Figs. 4.2 and 4.3. $(N_1)_{60}$ varies between 4 to 26 blows/ft throughout the dam. The upper 10 meters are loose with $(N_1)_{60}$ of less than 10 blows/ft particularly in the upstream or beach zones.

Fines Corrections for Liquefaction Triggering Analysis

Based on field data, Seed et al. (1984) had shown that the liquefaction resistance of sandy soils, at a given $(N_1)_{60}$ value, increases with increasing amount of fines in the soil (Fig. 4.4). Fines refers to materials passing the No. 200 sieve (i.e with average grain size of 0.075 mm or smaller). The measured $(N_1)_{60}$ values were corrected to account for the fines content of the tailings in Dashihe Dam. Figure 4.5 shows the average grain size distribution curves of tailings materials retrieved during the 1990 SPT soundings. The medium sands were considered "clean sands" with fines content of 5 % and therefore the $(N_1)_{60}$ values in

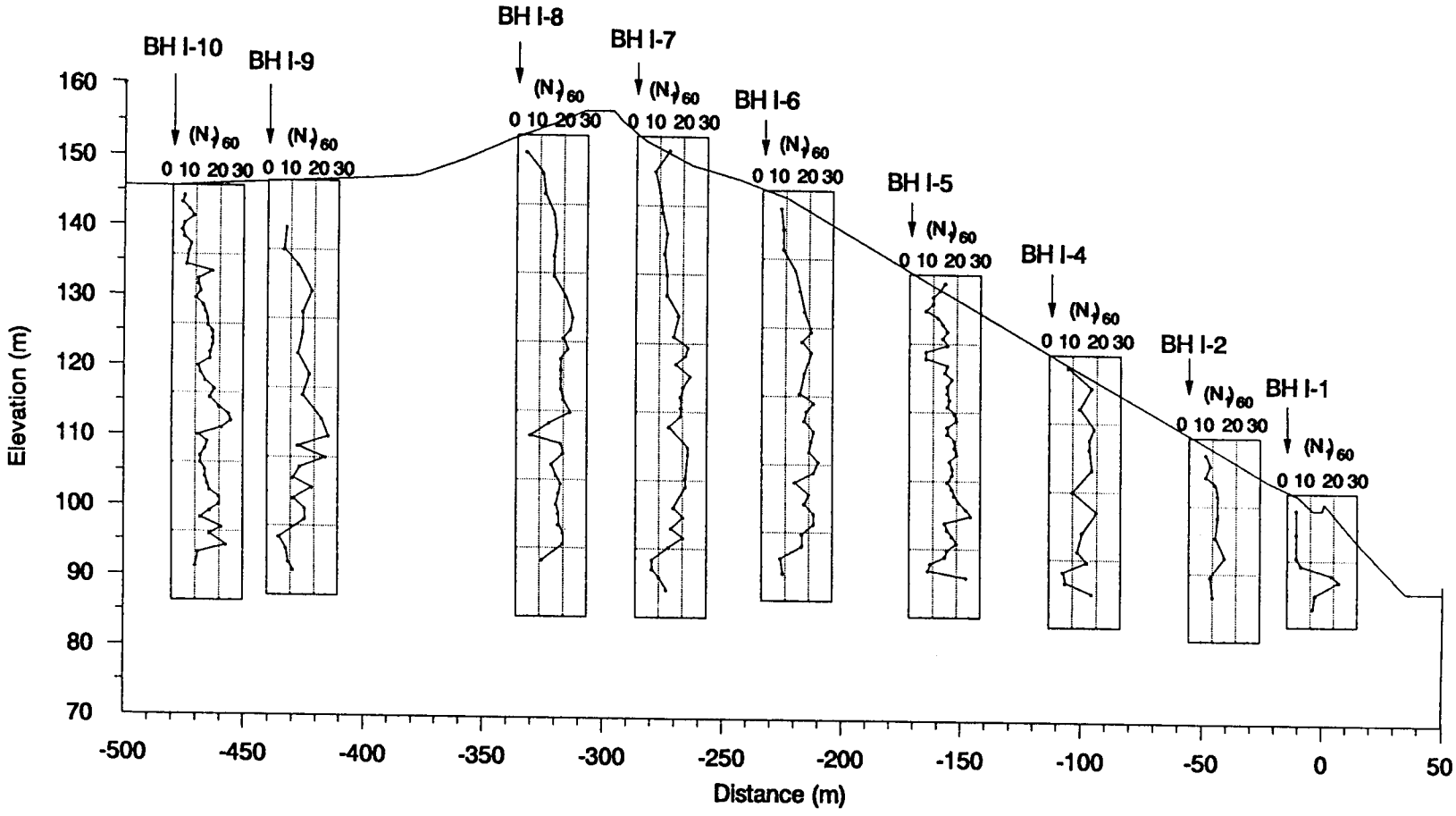

Fig. 4.2 - $(N_1)_{60}$ distribution in I-I cross-section of Dashihe Tailings Dam (1990)

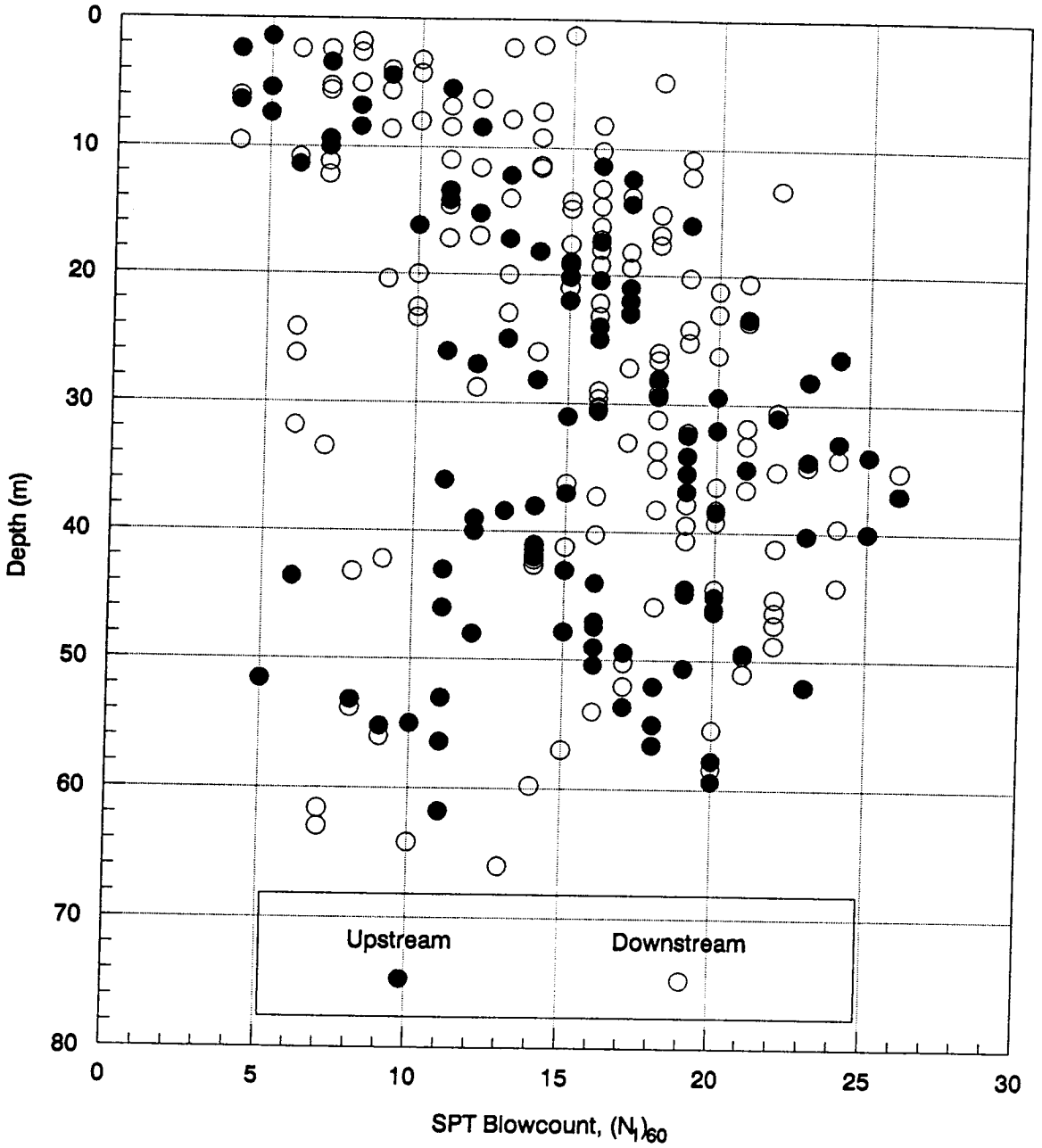

Fig. 4.3 - Dispersion of $(N_1)_{60}$ values in the 1990 Dashihe Dam

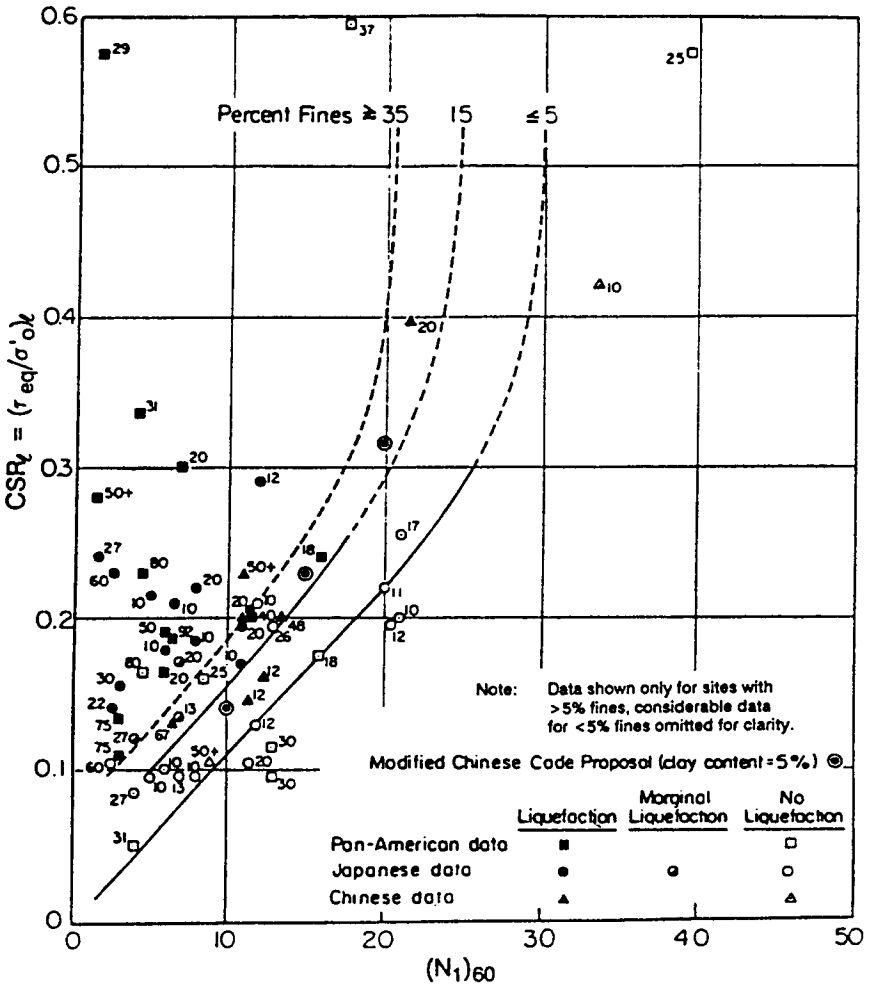

Fig. 4.4 - Relationship between cyclic stress ratios causing liquefaction and $(N_1)_{60}$ for M =7.5 earthquakes (After Seed et al., 1984)

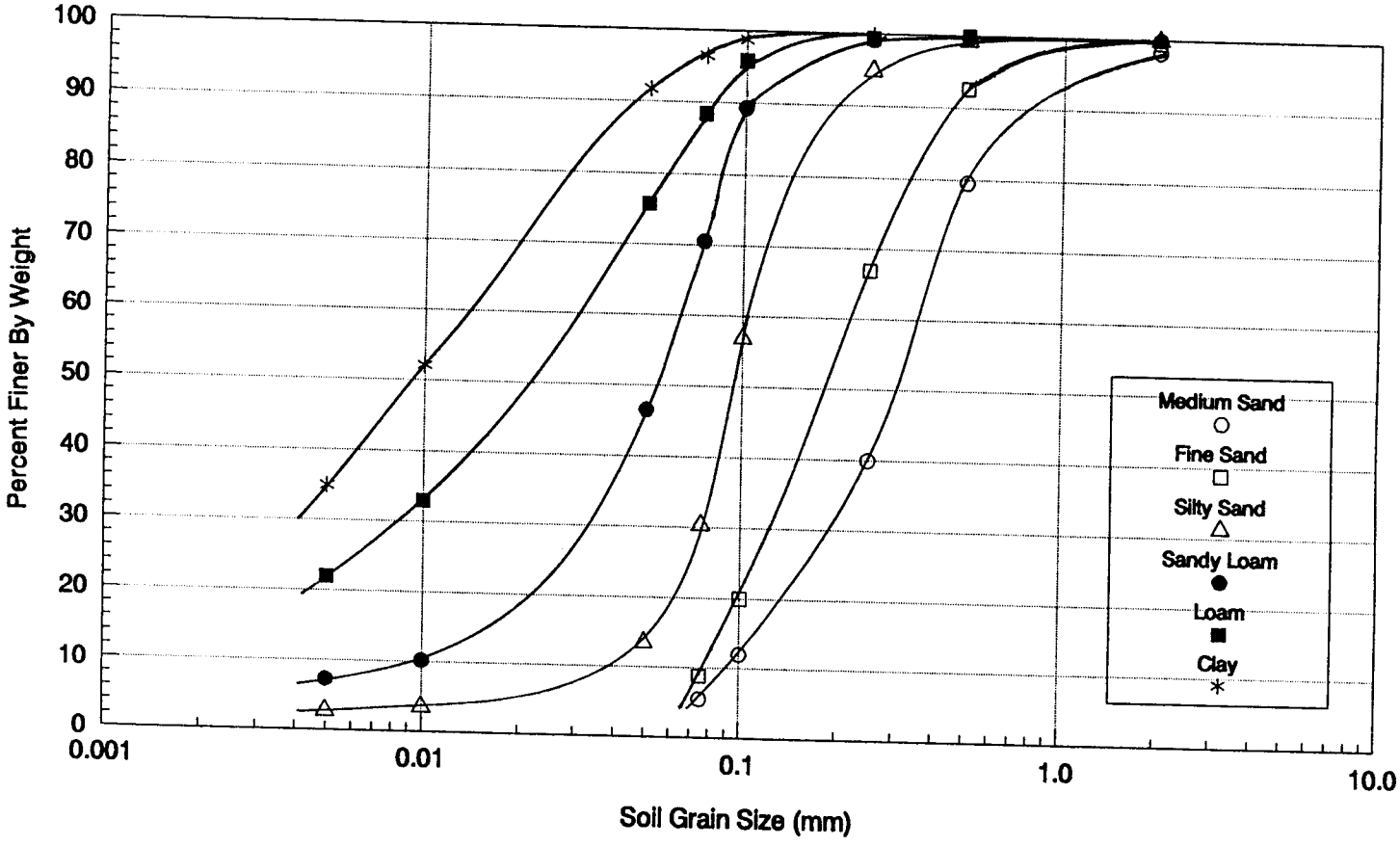

Fig. 4.5 - Average grain size distribution curves of Dashihe tailings materials obtained from SPT borings in 1990

these sands need not be adjusted. The fine sands had fines content of about 9 %, the silty sands had 30 %, and the sandy loam had 70 %. Therefore, the measured $(N_1)_{60}$ values of the fine sands were increased by 3 blows/ft while 7 blows/ft (the maximum possible increase) were added to the $(N_1)_{60}$ values of silty sands and sandy loam before using the liquefaction triggering chart by Seed et al. (1984).

Fines Corrections for Residual Strength Evaluation

An important aspect of the analysis of the seismic stability of an earth structure with potentially liquefiable materials such as a tailings dam is whether a flow failure will occur after liquefaction. This will depend on the relationship between the average driving shear stresses in the dam along any potential failure surface and the corresponding steady state or residual strengths of the liquefied materials (Castro et al., 1985). Accurate evaluation of in-situ residual strengths from laboratory testing has been shown to be a difficult task particularly for cohesionless soils (Vaid et al., 1989; Marcuson et al, 1990). Residual strengths (S_{ur}) derived from back analysis of several embankments that experienced flow failure during past earthquakes were correlated with $(N_1)_{60}$ values as shown in Fig.4.6 (Seed and Harder, 1990). This approach represents substantially the current state of practice for estimating the post-liquefaction strengths of sands.

Corrections of $(N_1)_{60}$ values for fines content have to be made before entering the correlation chart by Seed and Harder (1990) using Table 4.1. These corrections are different from those made when evaluating liquefaction potential. The $(N_1)_{60}$ of the fine sands and silty sands were increased by 1 and 2 blows/ft, respectively. Similarly, 5 blows/ft was added

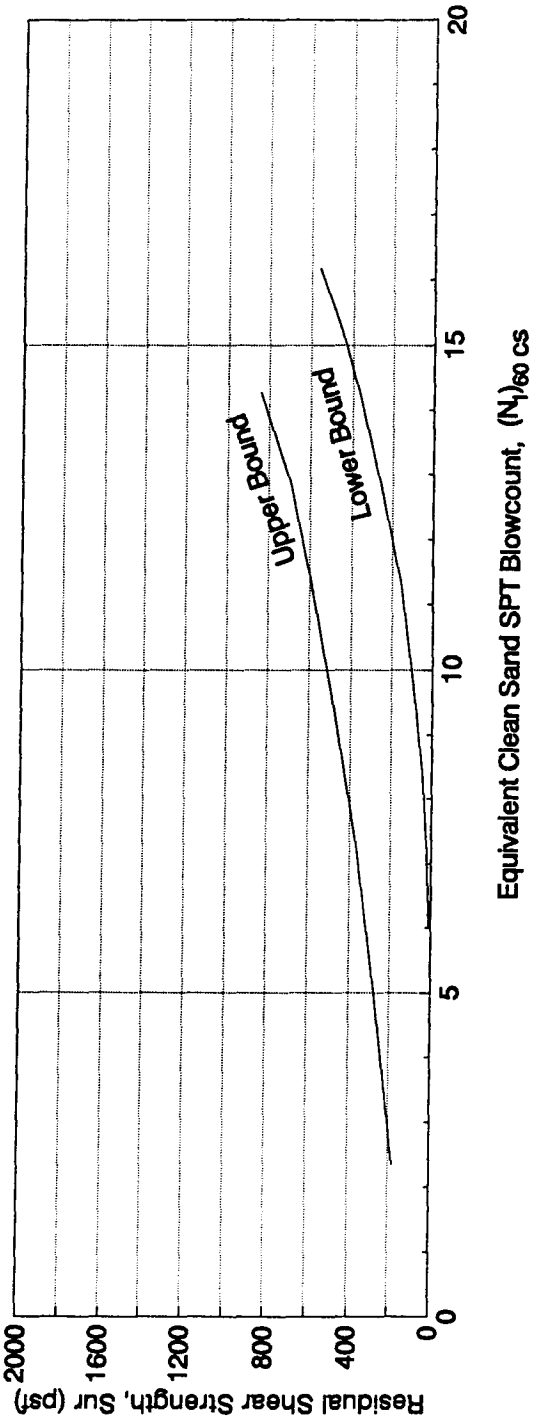

Fig. 4.6 - Relationship between residual strengths and $(N_1)_{60}$ values for clean sands (After Seed and Harder, 1990)

to the $(N_1)_{60}$ values of sandy loam and in-pond deposited slimes.

Table 4.1 - Fines corrections to measured $(N_1)_{60}$ for S_{ur} evaluation

Fines Content (%)	$\Delta\ (N_1)_{60}$ (blows/ft)
10	1
25	2
50	4
75	5

4.2 In-situ Shear Modulus Distribution

The distribution of in-situ dynamic shear moduli in the dam was determined from shear wave velocity measurements (Fig. 4.7) performed during the 1990 field exploration program at locations I-4, I-5, I-9 and II-6 (see Fig. 4.1).

The maximum shear modulus coefficient, $K_{2,max}$ which appears in the following equation (Seed and Idriss, 1970):

$$G_{max} = 21.7\ K_{2,max}\ P_a \left(\frac{\sigma'_m}{P_a}\right)^{1/2} \qquad (4.3)$$

was deduced from the field data and plotted against $(N_1)_{60}$ as shown in Fig. 4.8. The average relationship shown by the solid curve in Fig. 4.8 is used in assigning $K_{2,max}$ values for sandy soils in the dynamic response analysis of Dashihe Dam.

Figure 4.8 also shows that the average curve representing field data plots below the proposed formula by Seed et al. (1986) for estimating $K_{2,max}$ from $(N_1)_{60}$ of naturally

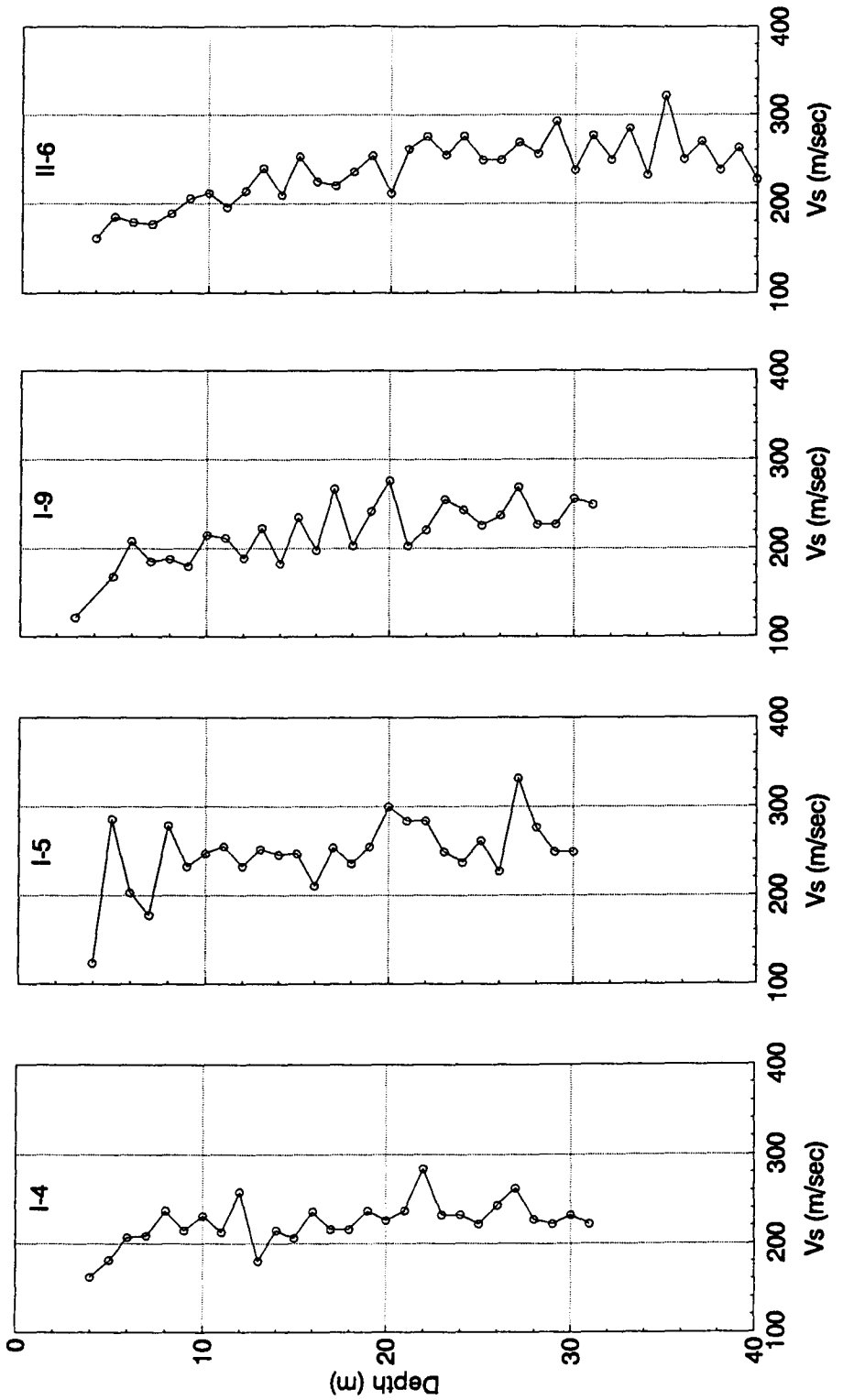

Fig. 4.7 - Shear wave velocities measured during seismic cone penetration tests in 1990

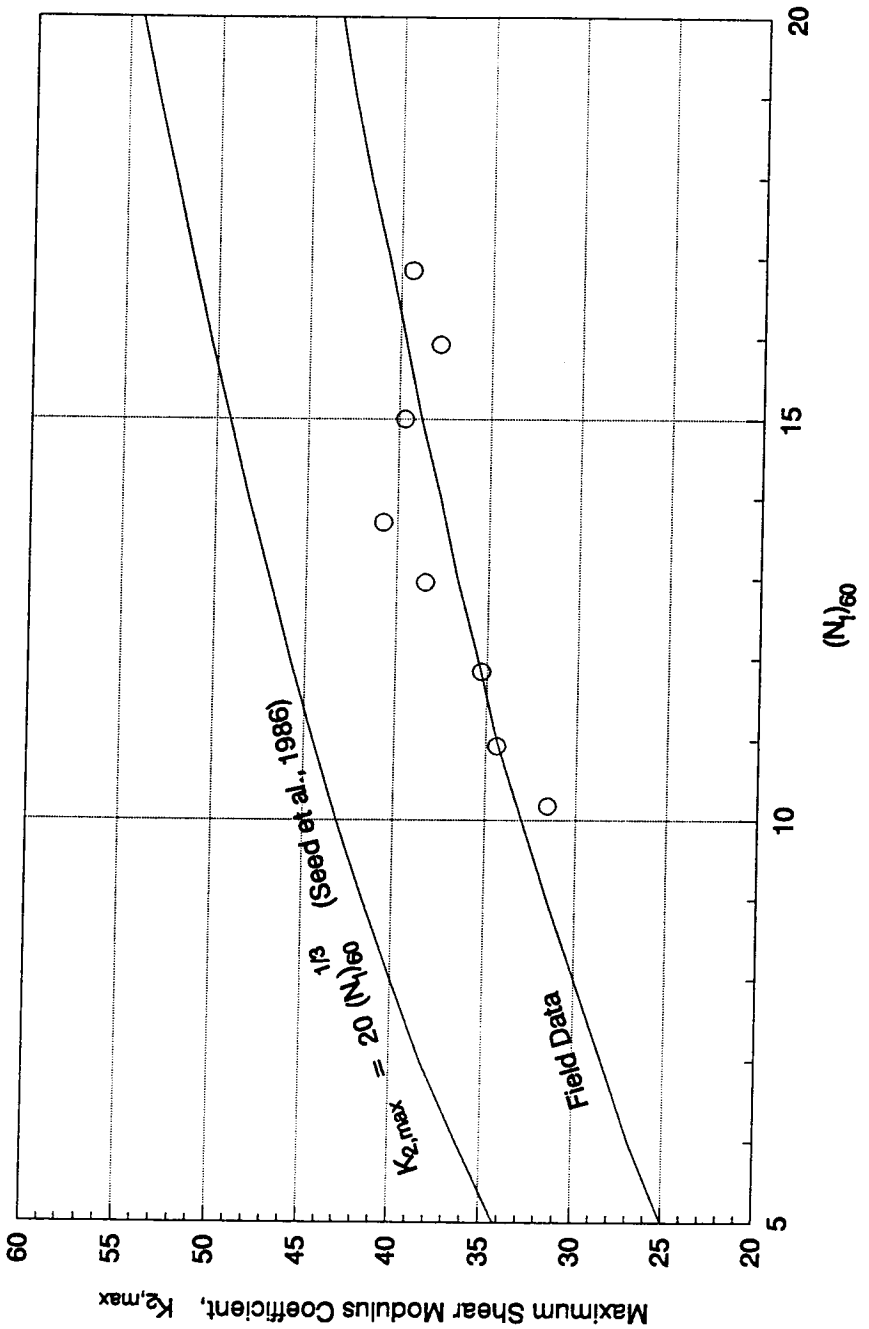

Fig. 4.8 - Relationship between $K_{2,max}$ and $(N_1)_{60}$

deposited sands given as follows:

$$K_{2,max} = 20\ (N_1)_{60}^{1/3} \qquad (4.4)$$

This indicates that the deposited tailings materials in Dashihe Dam have lower shear moduli, and thus, have lower resistances to dynamic shear-induced deformation than naturally deposited sands. The average $K_{2,max}$ in the field ranging from 25 to 43 as a function of $(N_1)_{60}$ shown in Fig. 4.8 bracket the value determined by Li et al. (1992) from SCPT data (Fig. 4.9).

4.3 Evaluation of Liquefaction Potential of Dashihe Dam Materials

The liquefaction resistance of the Dashihe Dam materials is estimated conservatively from Fig. 4.4 using the in-situ $(N_1)_{60}$ values. A correction for earthquakes of magnitude other than M = 7.5 is made by multiplying the resistance from Fig. 4.4 by a factor C_M given in Table 4.2. The number of equivalent uniform loading cycles N_L associated with different earthquake magnitudes can also be obtained from Table 4.2. The uniform cycles are assumed to have peak accelerations of 65 % of the maximum ground accelerations. Using Fig. 4.4 and Table 4.2, the conventional field liquefaction resistance curves can be derived for different $(N_1)_{60}$ values by plotting the different cyclic stress ratios associated with a particular $(N_1)_{60}$ value against the associated number of stress cycles to cause liquefaction. This procedure is illustrated in Fig. 4.10.

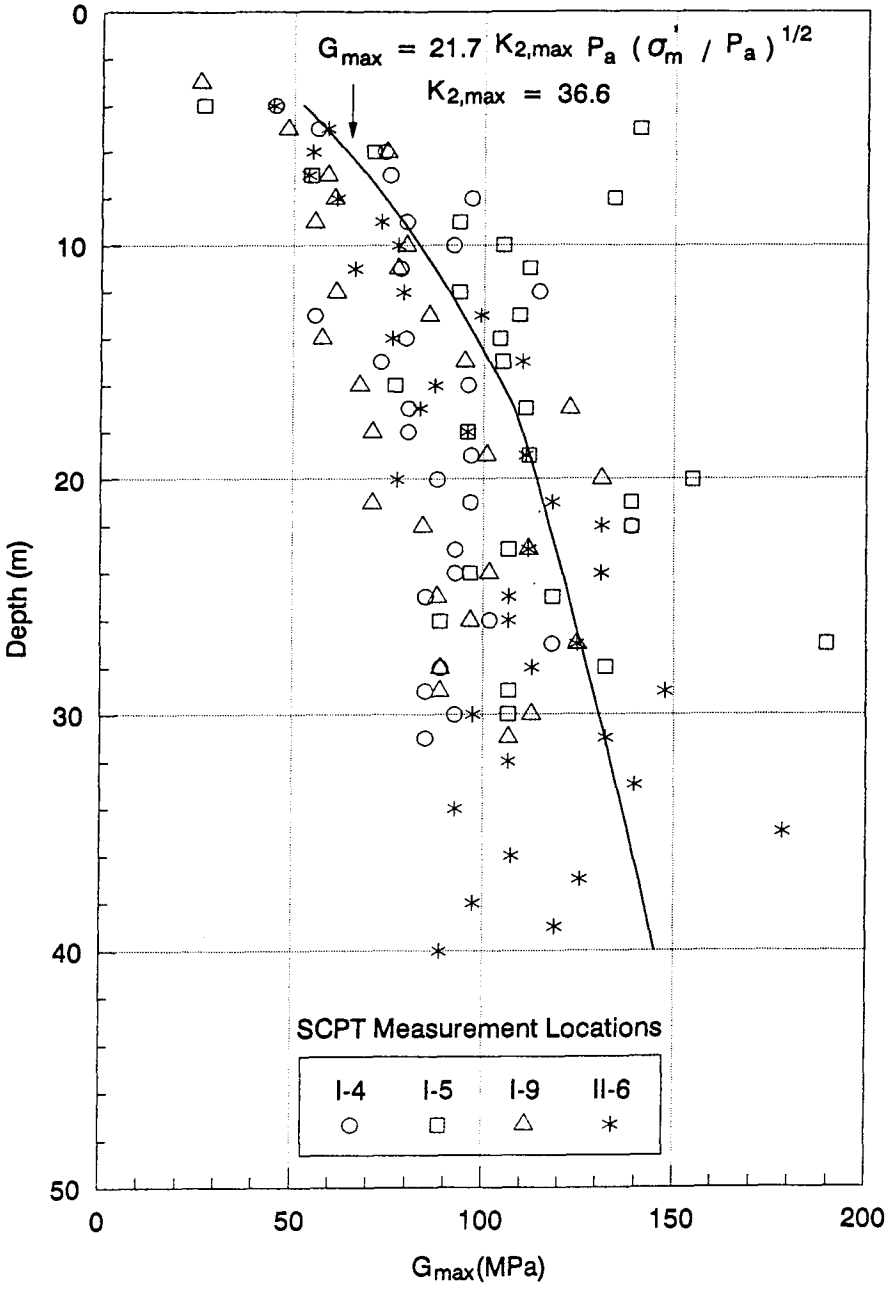

Fig. 4.9 - Determination of shear moduli from field SCPT data (After Li et al., 1992)

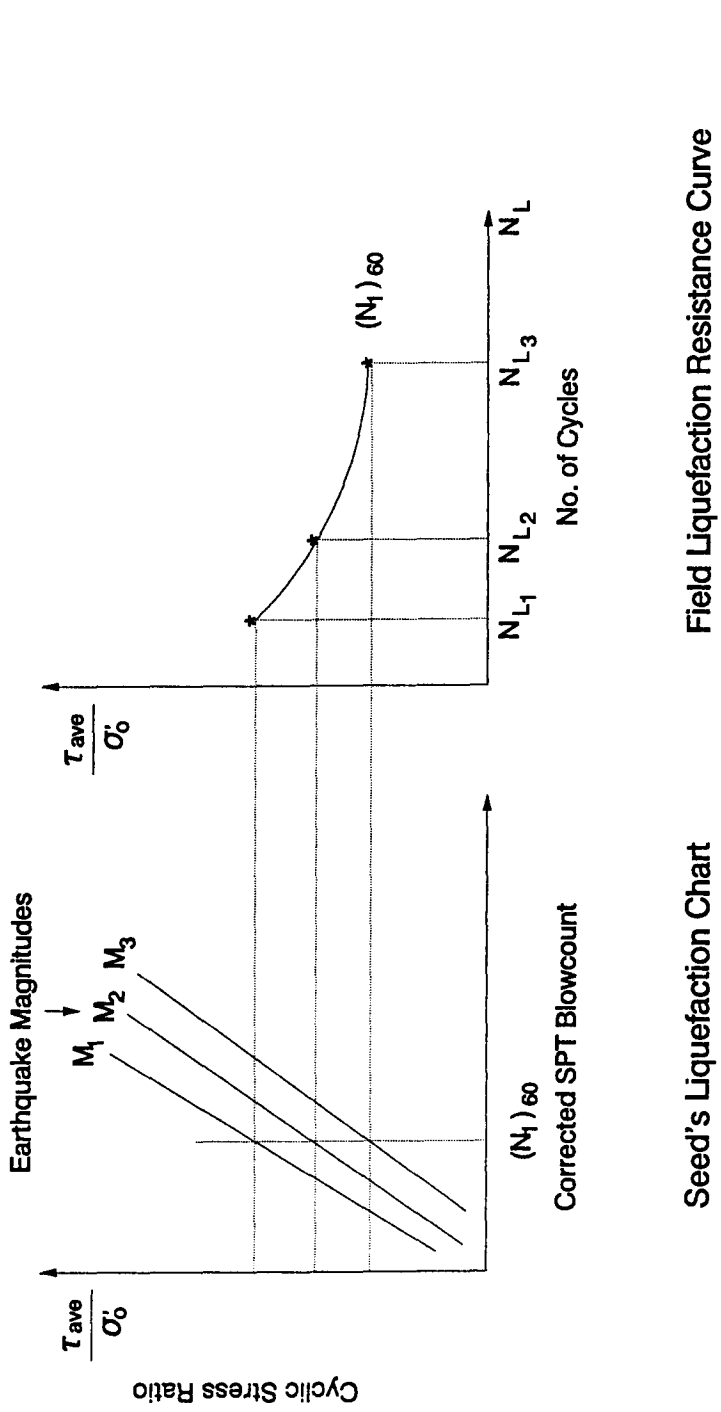

Fig. 4.10 - Derivation of field liquefaction resistance curve from Seed's liquefaction chart

Table 4.2 - Relationships among earthquake magnitude (M), number of equivalent uniform load cycles (N_L), and liquefaction resistance factor (C_M) (After Seed et al., 1984)

M	N_L	C_M
8.5	26	0.89
7.5	15	1.00
6.75	10	1.13
6.0	5-6	1.32
5.25	2-3	1.50

Liquefaction resistances obtained for typical material types and $(N_1)_{60}$ values found in Dashihe Tailings Dam are shown by the data points in Figs. 4.11 and 4.12 . The solid lines represent the liquefaction resistances computed using the porewater pressure model in TARA-3 (Finn et al., 1986). The constants C_1, C_2, m, n, and k_2 shown in the figures are the parameters in the model derived by curve-fitting analysis in SIMCYC2 program (Yogendrakumar and Finn, 1986). It is clear that a very close match with the field data can be obtained particularly at low $(N_1)_{60}$ values. Using field liquefaction resistance curves obtained from Fig. 4.4 is conservative because the curves represent lower bounds. However, this procedure is in accordance with the current engineering practice.

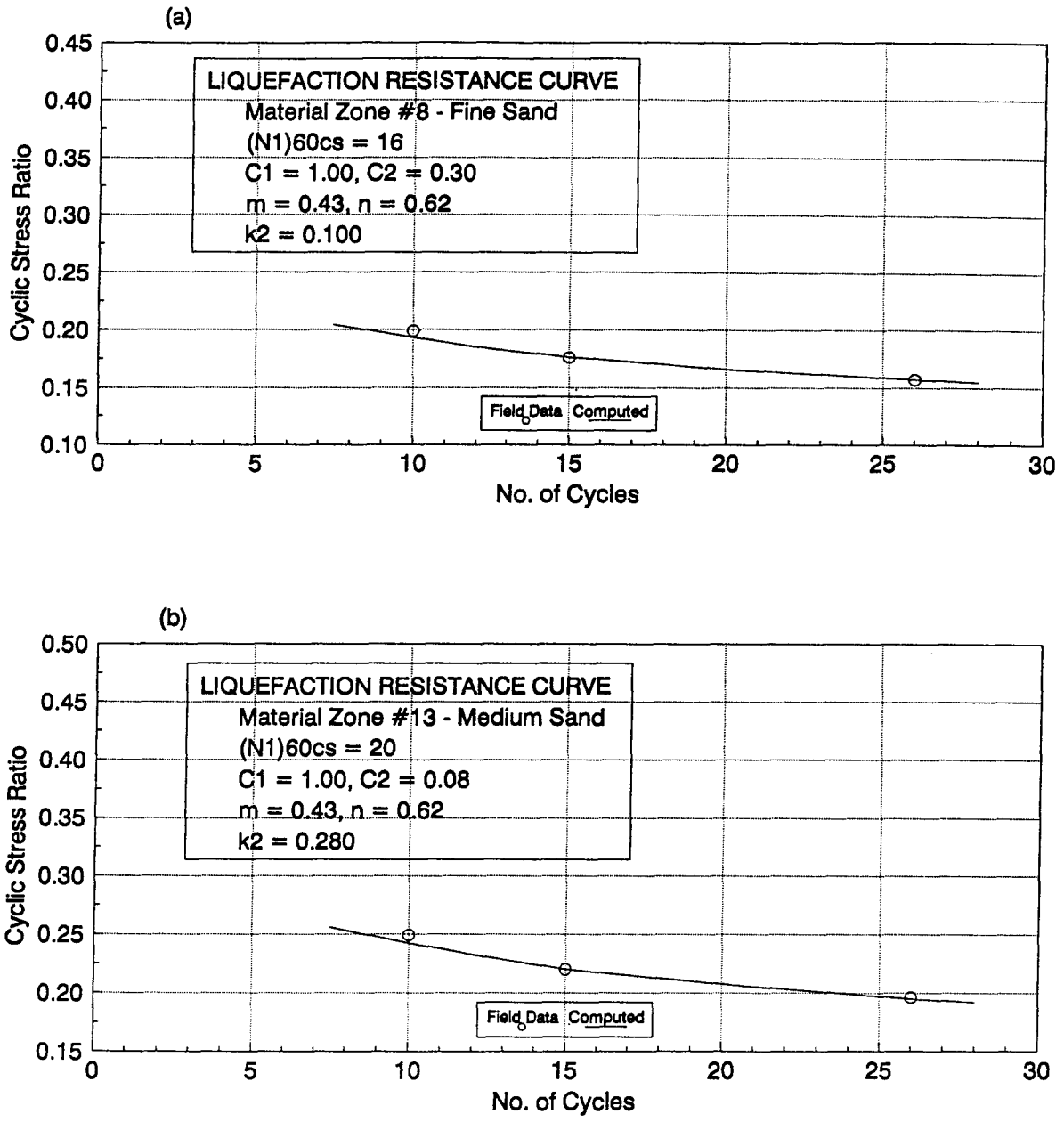

Fig. 4.11 - Liquefaction resistance curves for material zones #8 and #13

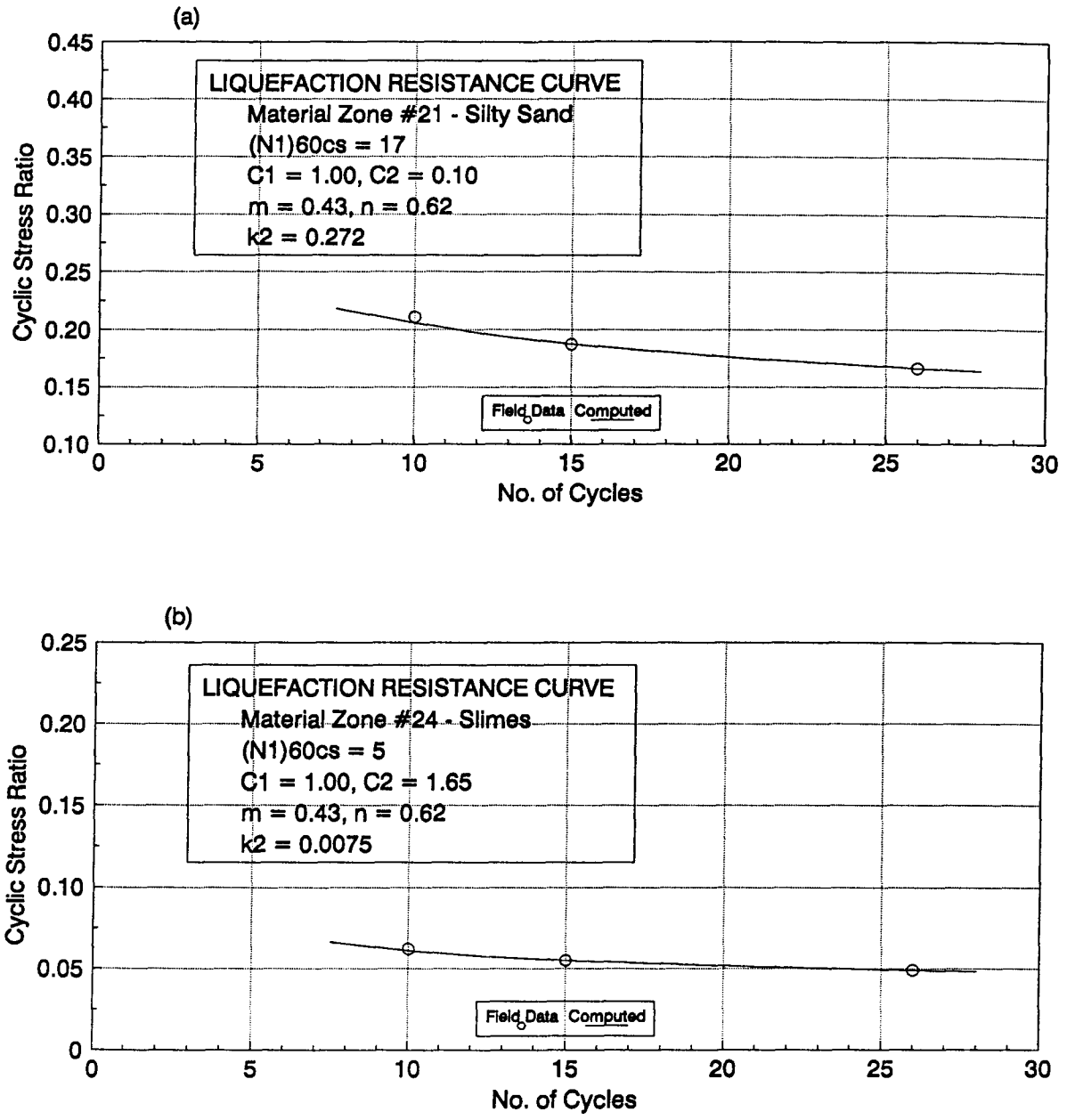

Fig. 4.12 - Liquefaction resistance curves for material zones #21 and #24

Chapter 5

SEISMIC RESPONSE ANALYSIS OF DASHIHE DAM (1990)

5.1 Nonlinear Effective Stress Analysis of Dams Using TARA-3 Program

The finite element program TARA-3 developed by Finn et al. (1986) has been used to assess the seismic response of a number of dams (e.g. Finn et al., 1987, Scott et al., 1989). Most recently, Finn and Xin (1992) used TARA-3 to simulate the seismic performance of the 1976 configuration of Dashihe Tailings Dam during the 1976 Tangshan Earthquake. Their analysis predicted the occurrence of liquefaction zones under the pond and beach and the development of cracking in the beach area and downstream shell. These results are in agreemeent with the phenomena observed after the earthquake and displayed the capability of TARA-3 to perform reliable estimation of the seismic capacity of Dashihe Tailings Dam as it increases in height. Accordingly, the seismic response and triggering of liquefaction for the 1990 configuration of Dashihe Dam is investigated using TARA-3. A description of TARA-3 is given in Appendix I.

5.2 Finite Element Mesh

The finite element mesh used to represent the main section (I-I) of Dashihe Tailings Dam is shown in Fig. 5.1. The mesh contains 661 nodes and 631 quadrilateral isoparametric elements. The dam cross-section is divided into 32 different material types reflecting different materials, the distribution of $(N_1)_{60}$ values, and the variation in effective confining pressure (Fig. 5.2). Material zones #1, #2 and #3 are nonliquefiable cohesive soils while

Node Numbers

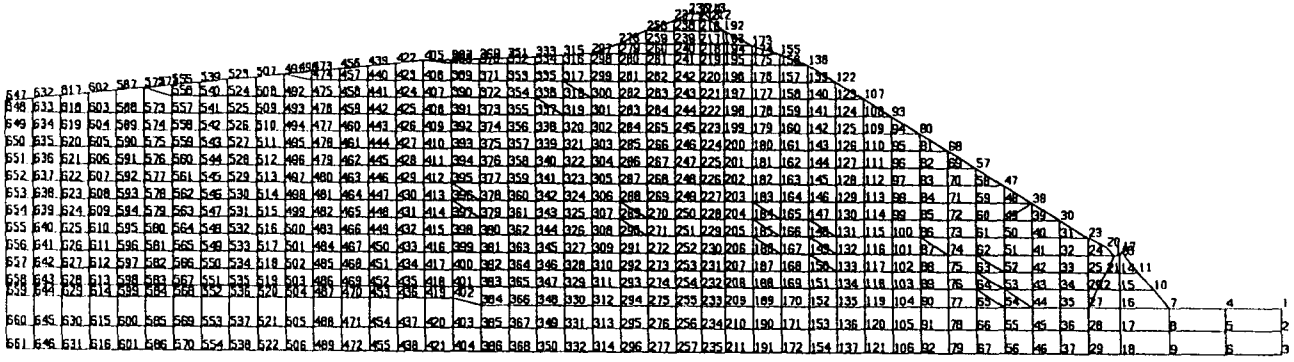

Element Numbers

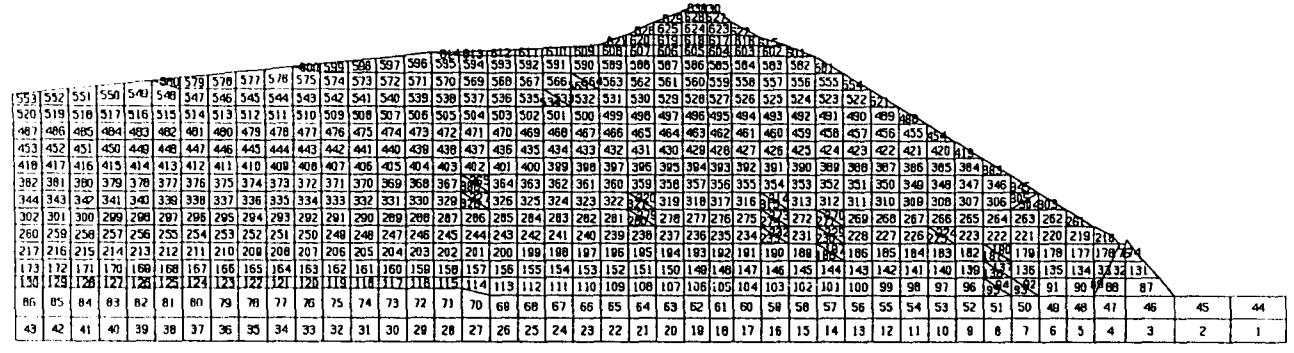

Fig. 5.1 - Finite element mesh representing the main cross-section of the Dashihe Tailings Dam (1990)

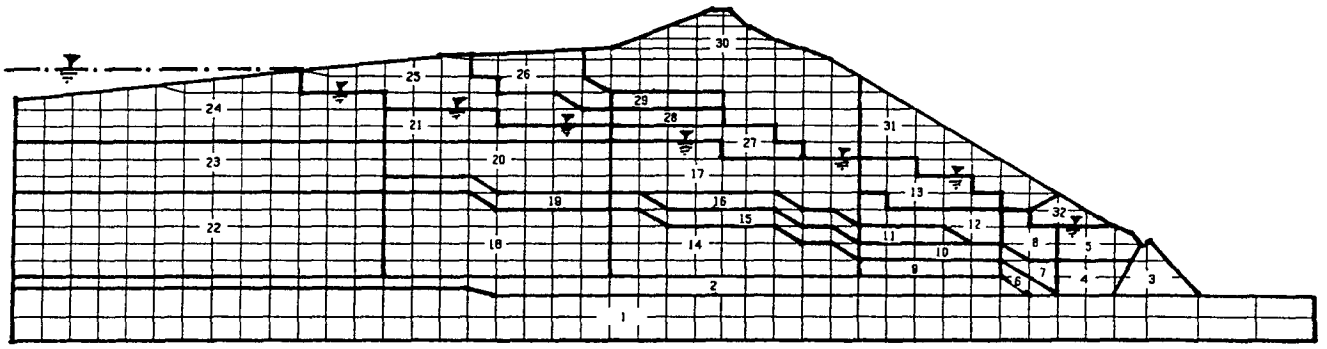

Zone #	Soil Type	Unit Weight kN/m3	Cohesion (kPa)	Friction Angle (deg)	(N1)60
1	Loam	19.4	312	0	
2	Clay	18.9	164	0	
3	Loam	20.7	100	0	
4	Silty Sand	19.8	0	35	6
5	Fine Sand	19.4	0	39	6
6	Sandy Loam	19.3	0	35	6
7	Silty Sand	19.8	0	35	10
8	Fine Sand	19.4	0	39	13
9	Sandy Loam	19.3	0	35	15
10	Silty Sand	19.8	0	35	15
11	Sandy Loam	19.3	0	35	15
12	Fine Sand	19.4	0	39	17
13	Medium Sand	19.9	0	39	17
14	Sandy Loam	19.3	0	35	15
15	Silty Sand	19.8	0	35	15
16	Sandy Loam	19.3	0	35	15
17	Fine Sand	19.4	0	39	19
18	Sandy Loam	19.3	0	35	13
19	Silty Sand	19.8	0	35	13
20	Fine Sand	19.4	0	39	12
21	Silty Sand	19.8	0	35	10
22	Slimes	19.8	0	35	7
23	Slimes	19.8	0	35	5
24	Slimes	19.8	0	35	5
25	Silty Sand	16.0	0	35	6
26	Fine Sand	15.7	0	39	7
27	Fine Sand	15.7	0	39	19
28	Silty Sand	16.0	0	35	15
29	Fine Sand	15.7	0	39	13
30	Medium Sand	16.1	0	39	11
31	Medium Sand	16.1	0	39	11
32	Fine Sand	15.7	0	39	9

Fig. 5.2 - Distribution of material types and soil properties in the 1990 Dashihe Dam

zones #4 to #24 consist of potentially liquefiable materials.

5.3 Dynamic Analysis of Dashihe Dam

The computed zones of liquefaction are indicated by the shaded areas in Fig. 5.3 for the input ground motions representative of the Luanxian Earthquake (M = 7.1) and the main shock of the Tangshan Earthquake (M = 7.8). Both earthquakes are found capable of generating liquefaction and high porewater pressures under the pond and the beach area near the pond. Liquefaction is also predicted to occur in a very limited portion of the downstream shell adjacent to the crest of the starter dam. Below the zone of liquefaction, the porewater pressures ranged from 80 % to 30 % of the effective overburden pressure with increasing depth. In the areas under the crest and the adjacent downstream slope, the seismically-induced porewater pressures are very low with values ranging from 1 % to 10 % of the effective overburden pressure.

The results show that the Tangshan earthquake shaking would develop more extensive liquefaction zone than the Luanxian earthquake despite of the fact that its peak input acceleration is 50 % less. Finn and Xin (1992) obtained similar results in their analysis of the 1976 section of the Dashihe Dam.

The ratios of maximum surface acceleration response to maximum input base motion or amplification factors are calculated and compared for both earthquakes at different locations over the entire section of the 1990 Dashihe Dam being analyzed (Fig. 5.4). The amplification factors for the Tangshan earthquake are greater than those obtained for the Luanxian earthquake over the entire section of the dam with a maximum value of about 2.0

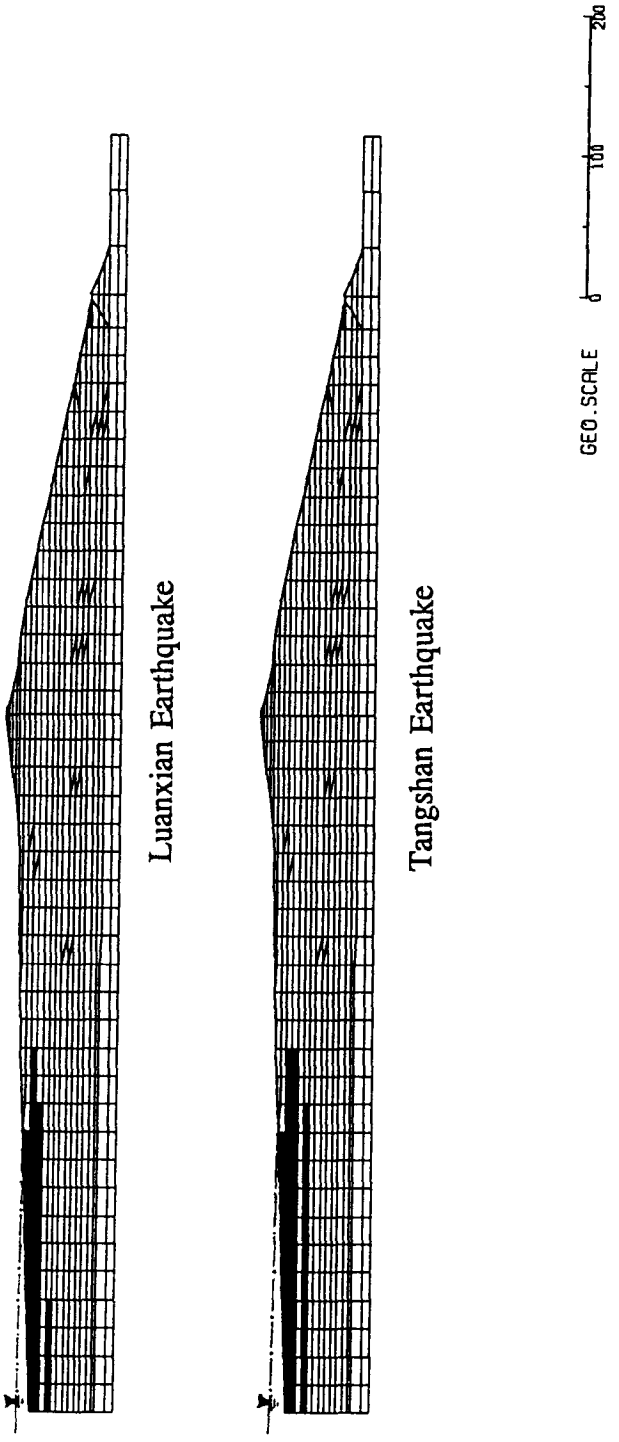

Fig. 5.3 - Computed liquefied zones (indicated by shaded areas) in Dashihe Dam generated by Tangshan and Luanxian earthquakes

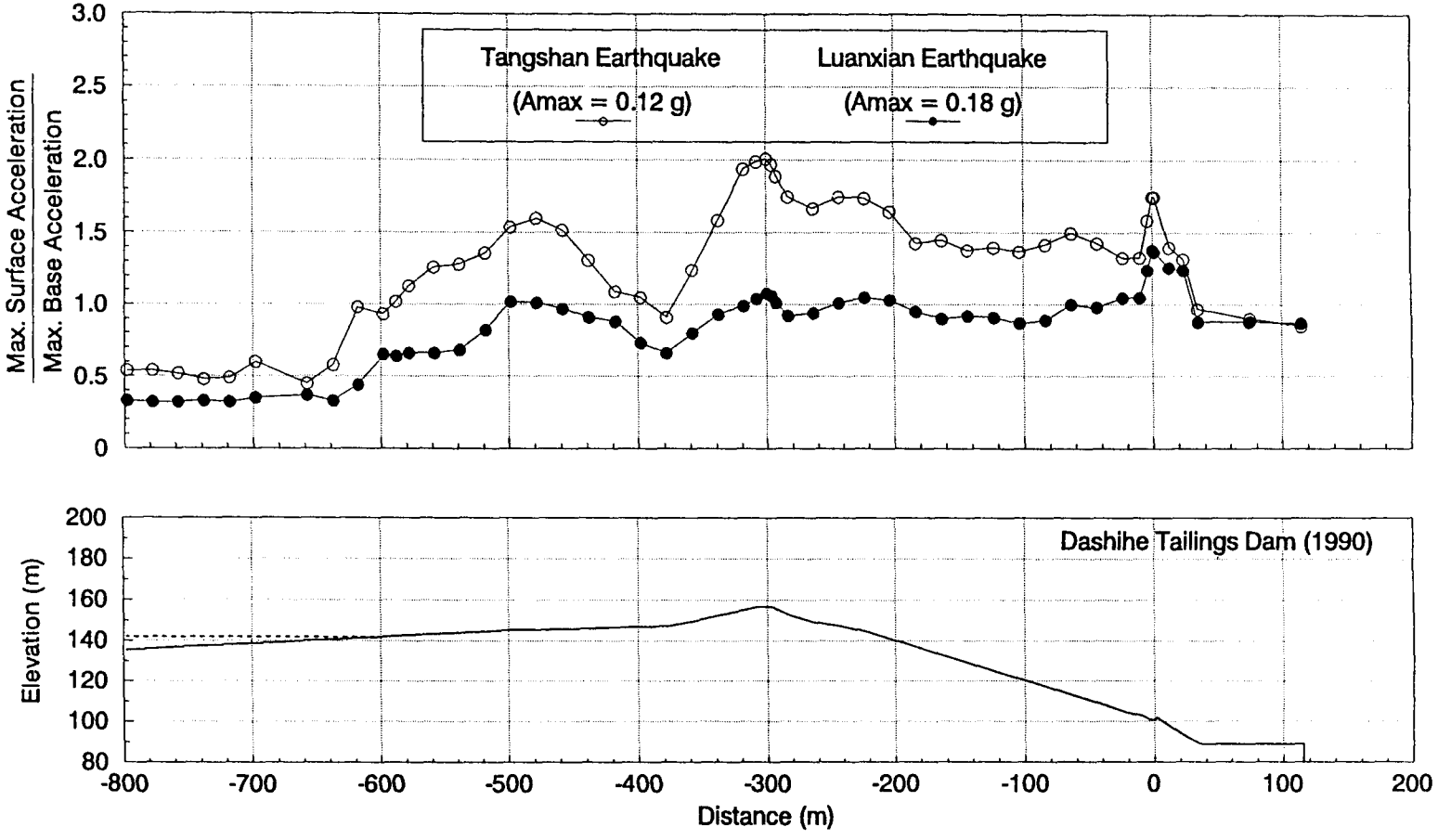

Fig. 5.4 - Computed amplification factors for Tangshan and Luanxian earthquakes

occurring at the crest of the dam. It is interesting to observe the effects of surface topography on seismic response from Fig. 5.4. The curves of amplification factors follow the same shapes over the entire section of the dam. The amplification factor rises rapidly as the crest of a ridge is approached. On the other hand, the amplification factor declines sharply as the flat beach is approached. This phenomenon had been observed in many field studies (e.g. PWRI, 1986; Celebi and Hanks, 1986) and theoretically investigated by Aki (1988) and Faccioli (1991).

In general, there is no significant amplification of maximum input motions for the Luanxian earthquake except at the crest and the external slope of the starter dam. In both cases, substantial deamplification of motions occurred at locations where liquefaction and high porewater pressures developed indicating the effects of porewater pressures on seismic response.

The influence of porewater pressures on seismic response can be illustrated by examining the shear stress-strain response at various porewater pressure levels. Figure 5.5 shows the time histories of porewater pressure build-up due to the Tangshan earthquake at selected locations along a vertical section passing through the liquefied zone under the beach. Soil element #541 liquefied during the early stage of seismic excitation, i.e. after about 7 seconds. When liquefaction developed in element #541, the shear stresses dropped to negligible values (Fig. 5.6a). The materials suffered severe softening and strength loss with most of the resistance to seismic straining resulting from damping as shown by the degraded stress-strain hysteresis loops in Fig. 5.6b.

The porewater pressure ratio in element #441 achieved a peak value of 75 % in the

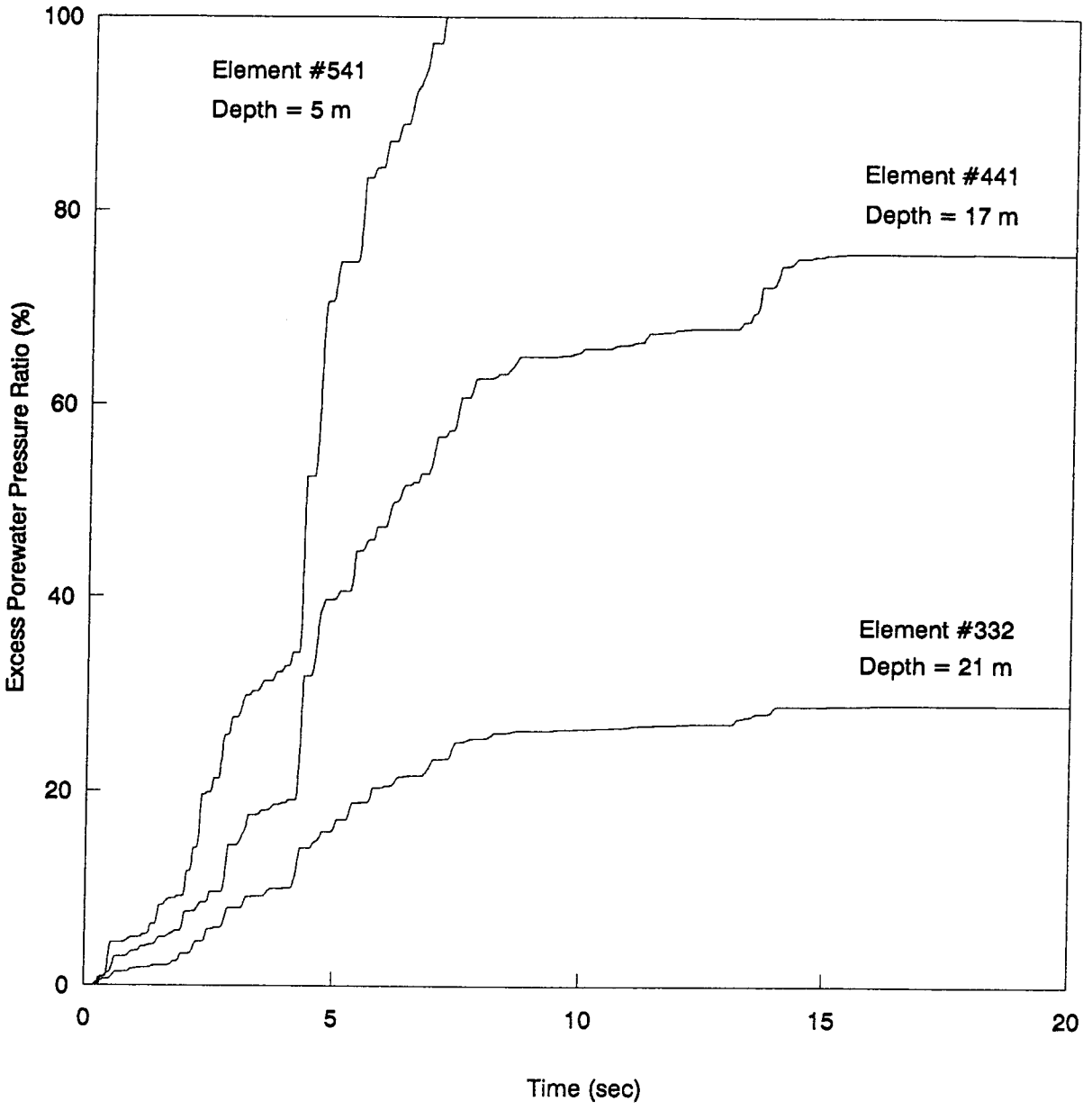

Fig. 5.5 - Porewater pressure time histories in elements #541, #441 and #332 (Tangshan Earthquake, 1976)

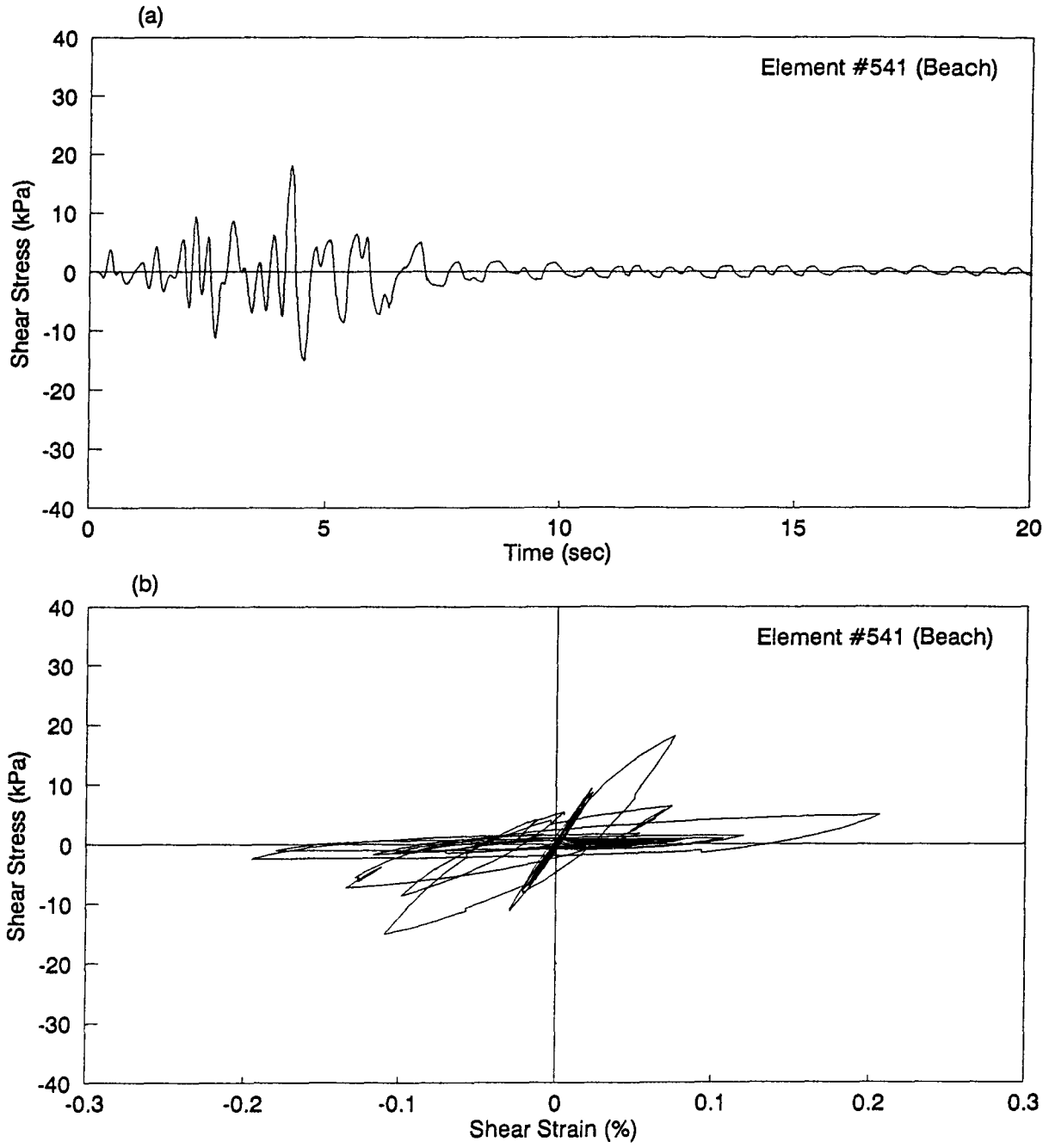

Fig. 5.6 - Shear stress time history and stress-strain response in element #541 in Dashihe Dam (1990) (Tangshan Earthquake, 1976)

later stage of shaking (Fig. 5.5). The progressive increase in porewater pressure is accompanied by the gradual reduction in the shear stress amplitudes with time, but unlike in element #441, significant values of shear stresses are transmitted (Fig. 5.7a). The corresponding hysteresis loops increase in area and the average slope gradually decreases (Fig 5.7b). This behavior is characteristic of increased damping and stiffness degradation associated with the reduction in effective stresses caused by the seismic porewater pressures.

In element #332, located far down below the liquefied layer, the porewater pressures are generated at a slower rate reaching a maximum value of 29 % of the effective overburden pressure towards the end of shaking (Fig. 5.5). Due to lower porewater pressure development, relatively larger values of shear stresses could be transmitted in this element compared with element #441 (Fig. 5.8a). The slope of the entire stress-strain loop for element #332 is almost unchanged indicating nearly elastic response allowing the material to transmit large shear stresses at small strains (Fig. 5.8b).

The computed accelerations and dynamic displacements at node #456, located on the beach surface above the liquefied zone, are shown in Fig. 5.9. Notice the reduction in both the frequency and amplitude of accelerations at node #456 after about 7 seconds, consistent with the fact that the underlying materials (element #541) liquefied after 7 sec and were therefore too weak in shear to transmit significant accelerations from below. Figure 5.9 shows the eventual accumulation of permanent displacements as a result of the shaking. Note that these displacements do not include the flow deformations due to the effects of gravity on the weakened material. The flow deformations will be discussed in the next chapter.

The computed accelerations and displacements at the crest of the dam (node #214)

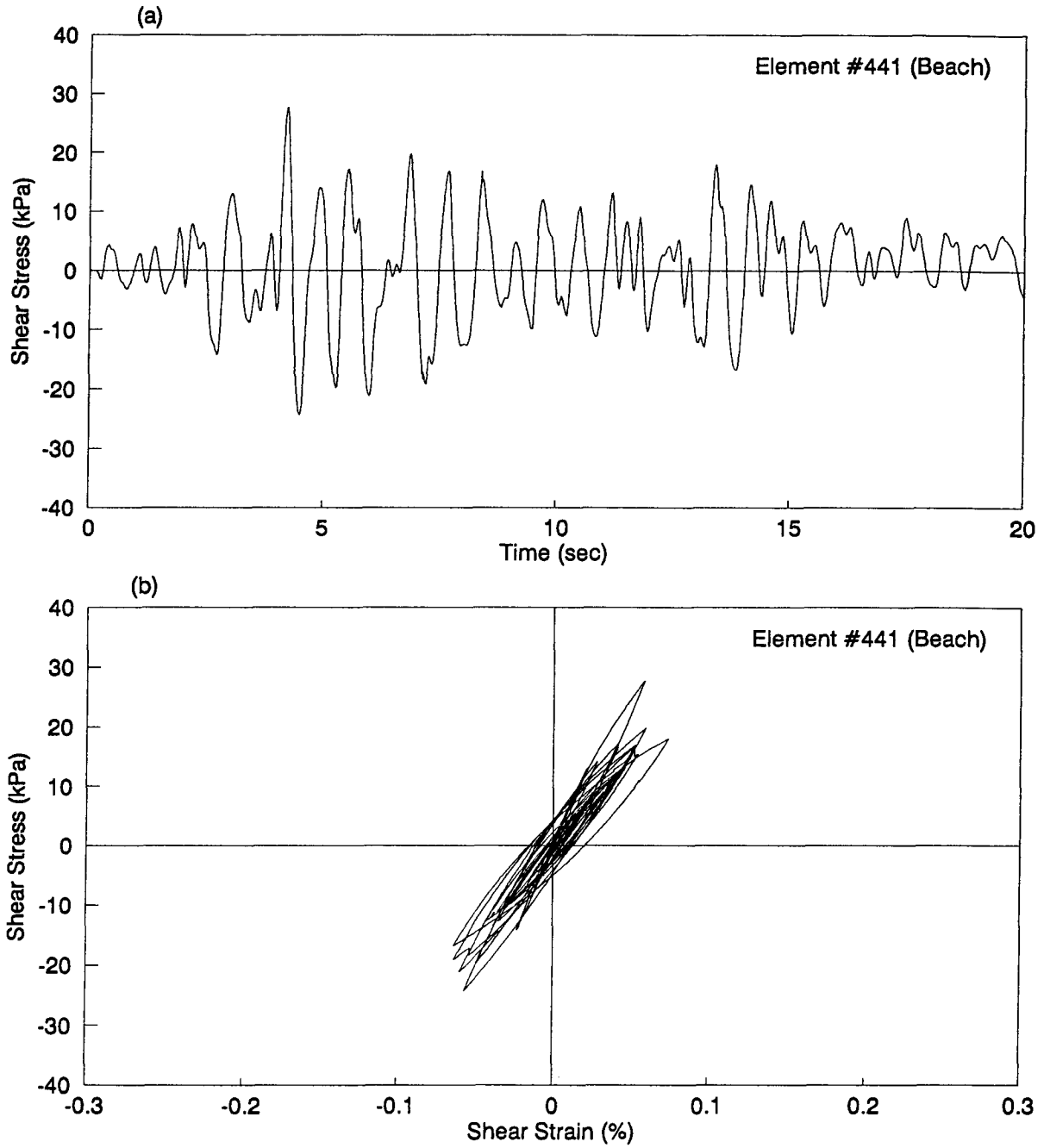

Fig. 5.7 - Shear stress time history and stress-strain response in element #441 in Dashihe Dam (1990) (Tangshan Earthquake, 1976)

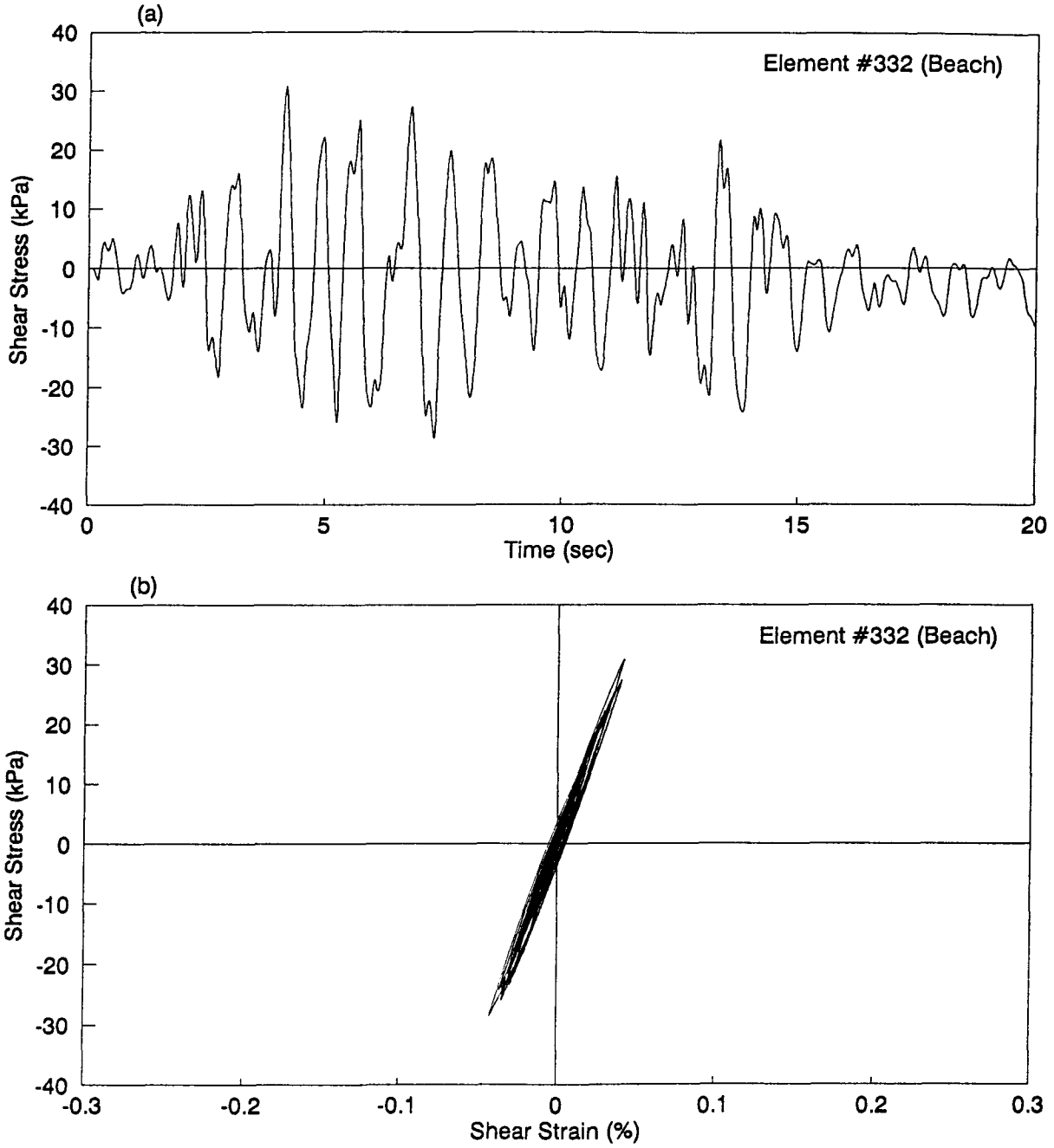

Fig. 5.8 - Shear stress time history and stress-strain response in element #332 in Dashihe Dam (1990) (Tangshan Earthquake, 1976)

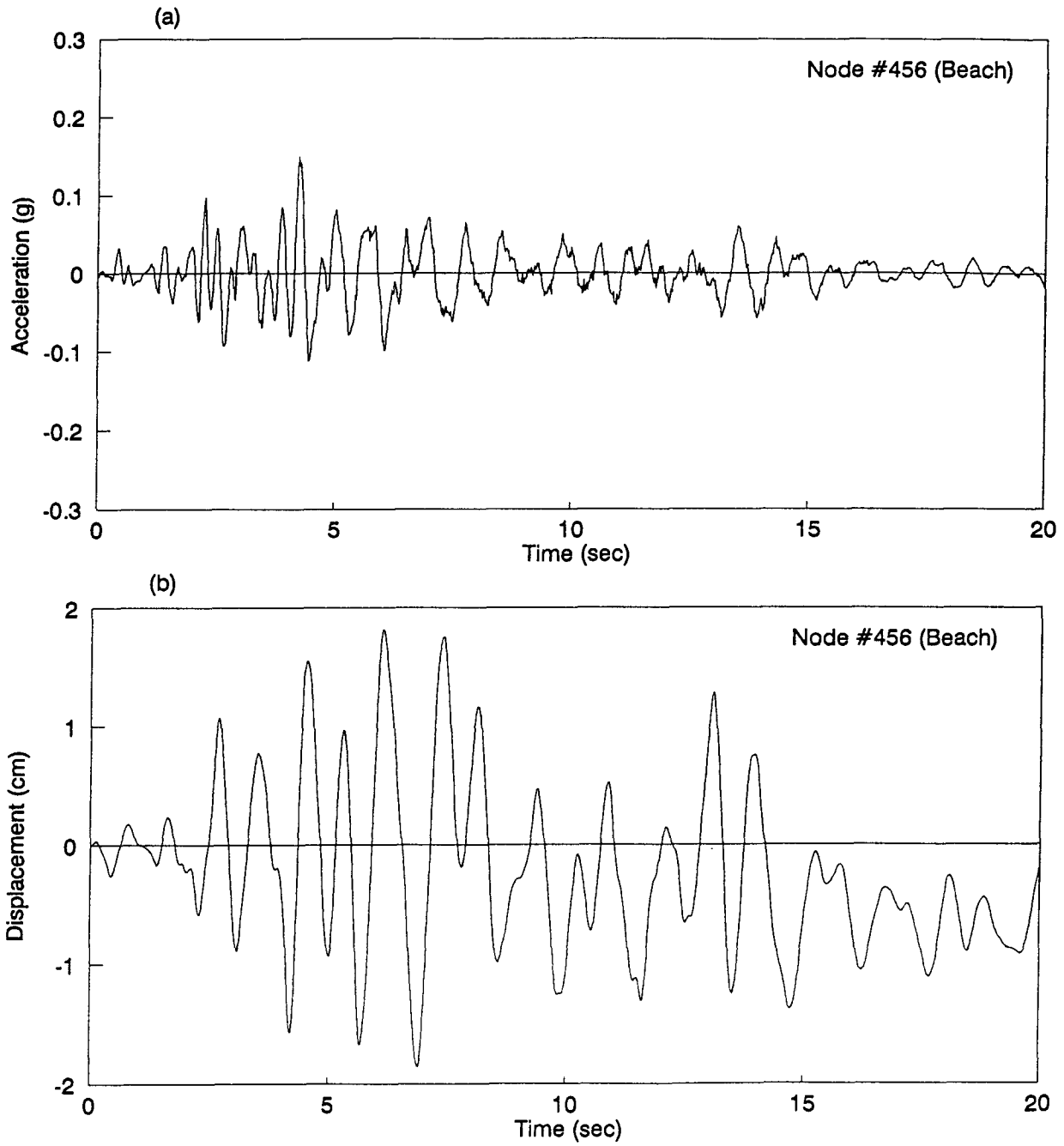

Fig. 5.9 - Acceleration and displacement response at node #456 in Dashihe Dam (1990) (Tangshan Earthquake, 1976)

and a surface node on the downstream shell (node #68) are shown in Figs. 5.10 and 5.11, respectively. The accelerations at the crest of the dam reached a maximum value of about 0.24 g, which is twice as large as the maximum base excitation. This result is consistent with the low porewater pressures generated under the crest and the adjacent downstream slope. The dynamic displacements in these areas indicate a mainly elastic response with no significant residual displacements.

During the earthquake in 1976, extensive cracking occurred in the beach area parallel to the dam axis. These cracks were found parallel to each other and measured about 20-700 mm in width, 10-30 m in length and up to 1 m in depth. The closer to the pond, the denser became the concentration of these cracks. These cracks could be caused by the development of dynamic tensile stresses in the beach area during the earthquake. Finn and Xin (1992) verified this in their analysis of the 1976 section of the dam by examining the time variation in horizontal normal stresses in surface elements at the locations where they were observed.

The possibility of crack formation for the 1990 section of the dam as a result of tensile development due to seismic shaking was also investigated. The time histories of horizontal normal stresses in surface elements in the entire stretch of the beach from the edge of the pond to the crest of the dam were retrieved from dynamic analysis and examined. Element #598 located close to the pond, and element #612 located 100 m away are representative of this area. The results for these elements, presented in Fig. 5.12, show that a number of stress cycles reach very low compressive values of about 2 kPa. These values are limiting values used in the program TARA-3 to prevent tension development. Stresses which reach these limiting values will in reality become tensile if the material could take

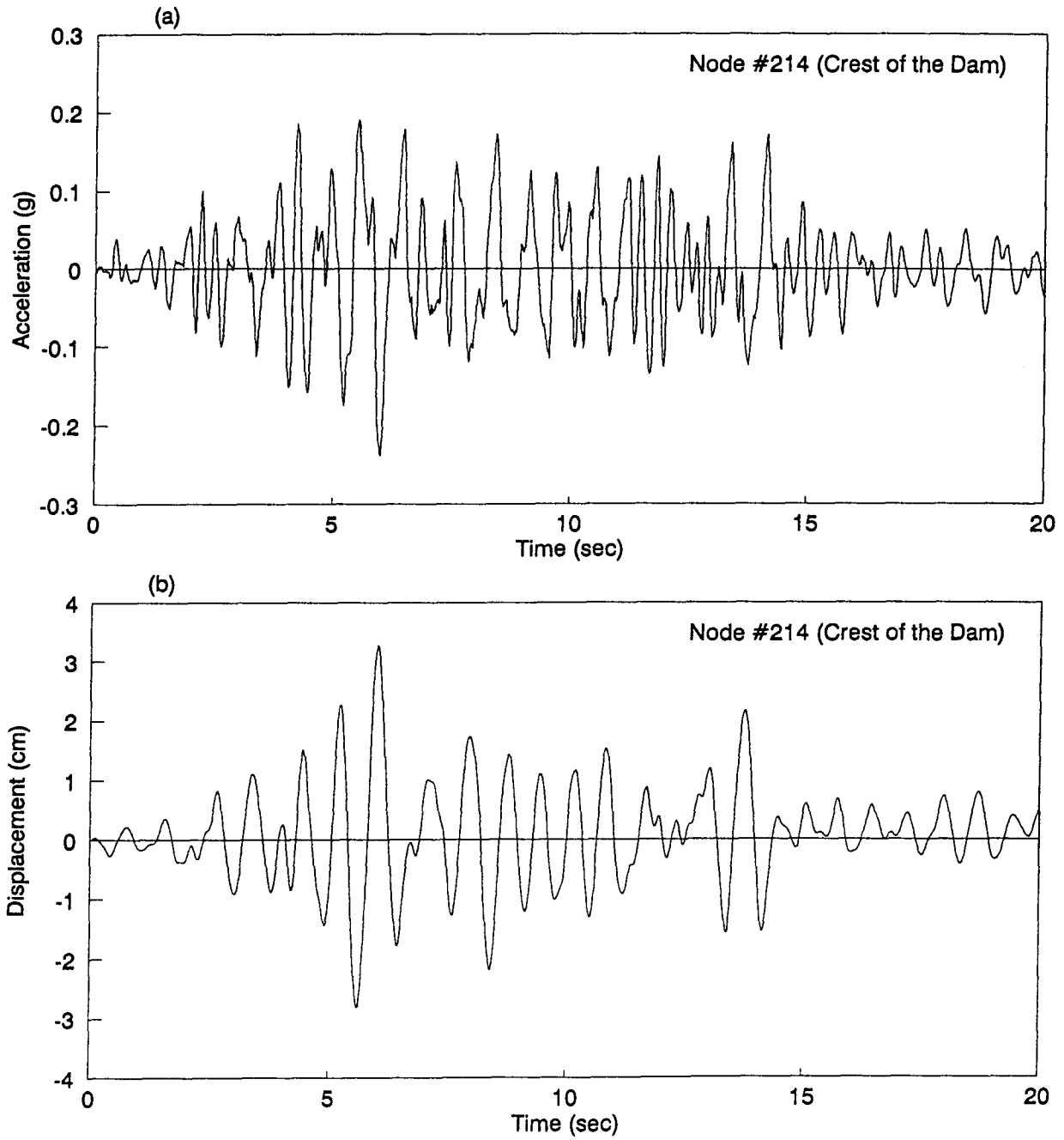

Fig. 5.10 - Acceleration and displacement response at node #214 in Dashihe Dam (1990) (Tangshan Earthquake, 1976)

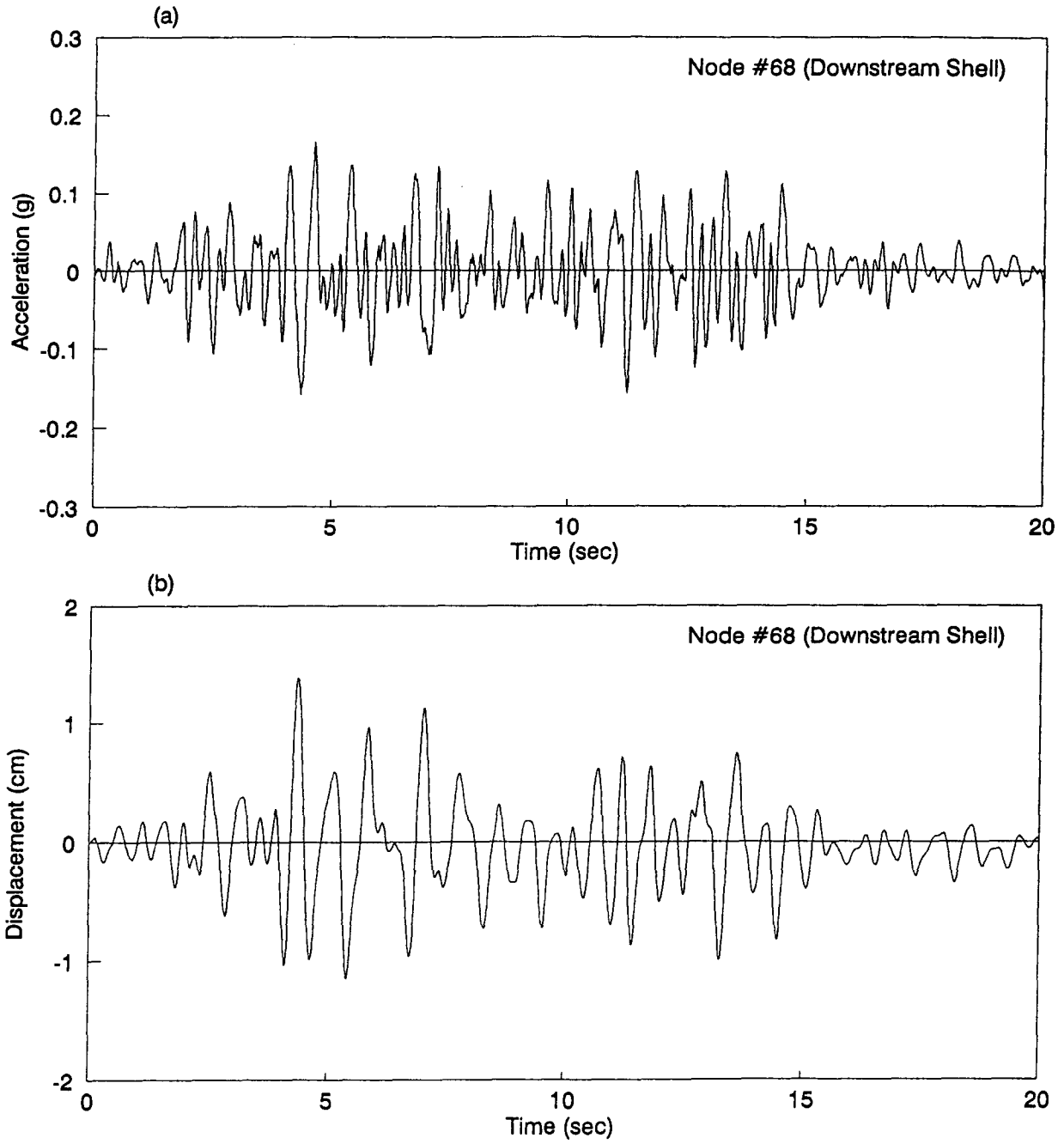

Fig. 5.11 - Acceleration and displacement response at node #68 in Dashihe Dam (1990) (Tangshan Earthquake, 1976)

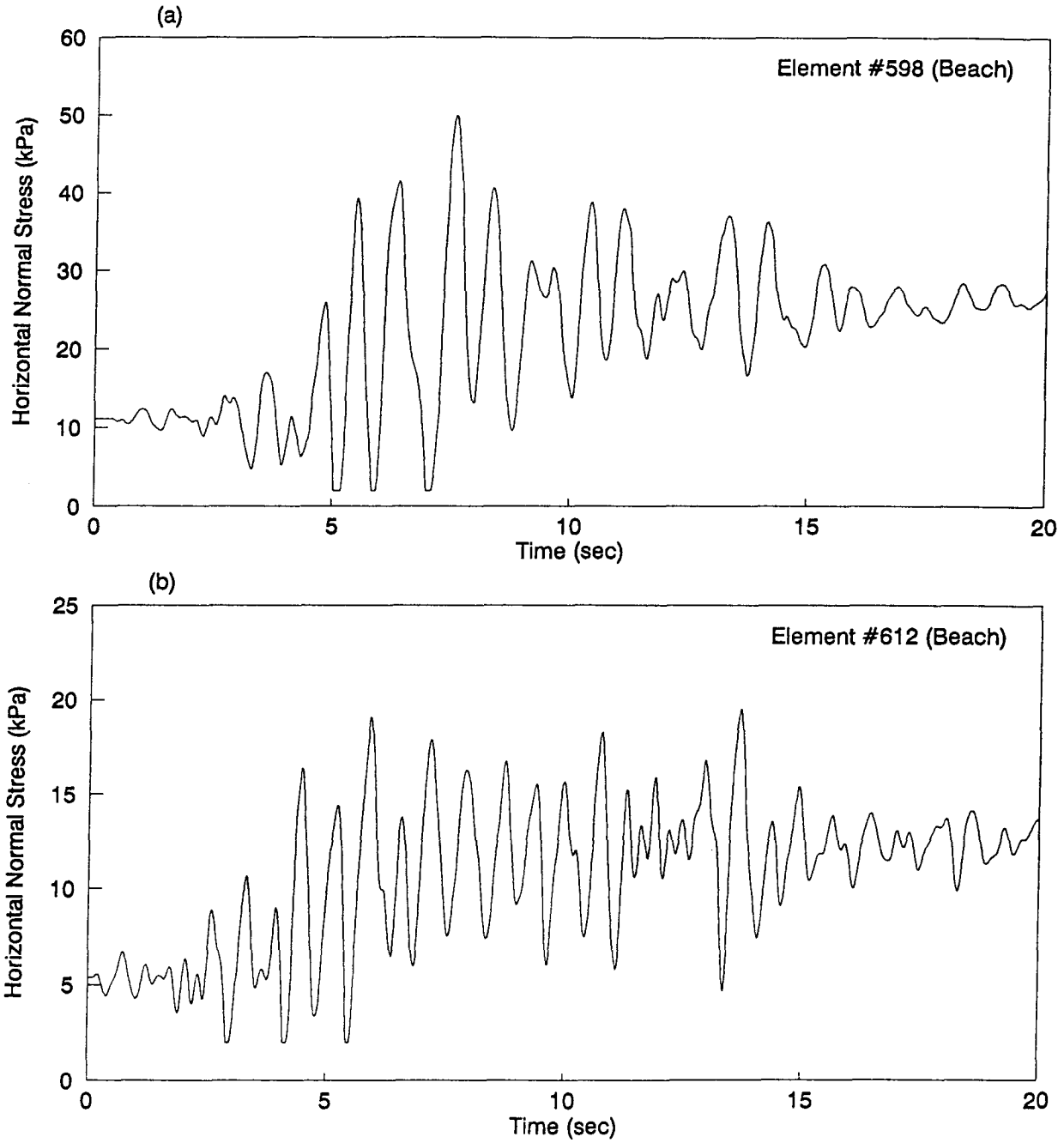

Fig. 5.12 - Horizontal stresses in elements #598 and #612 in Dashihe Dam (1990) (Tangshan Earthquake, 1976)

tension, otherwise cracking will develop. These cracking stresses occurred just before the liquefaction.

If the dam would be shaken by an earthquake equivalent to the main shock of the 1976 Tangshan event, cracking is predicted to occur in the beach from the edge of the pond up to a distance of about 160 m in the direction of the crest. Based on the observed performance of the dam during the 1976 earthquake, surface manifestation of liquefaction such as sand boils and water spouts could occur in the portion of the beach close to the pond where liquefaction and high porewater pressures are anticipated.

The possibility of cracking in the downstream shell was also investigated. Typical results, presented in Fig. 5.13, indicate that no cracking is expected to occur in the 1990 section of the dam if the same earthquake should take place. However, liquefaction would develop in surface element #218 located near the crest of the starter dam at about the same location where minor cracking was observed during the 1976 earthquake. Such localized liquefaction of surface materials was not observed during the 1976 earthquake because the phreatic surface elevation just before the 1976 earthquake was much lower and did not reach the crest of the dam as it did in 1990.

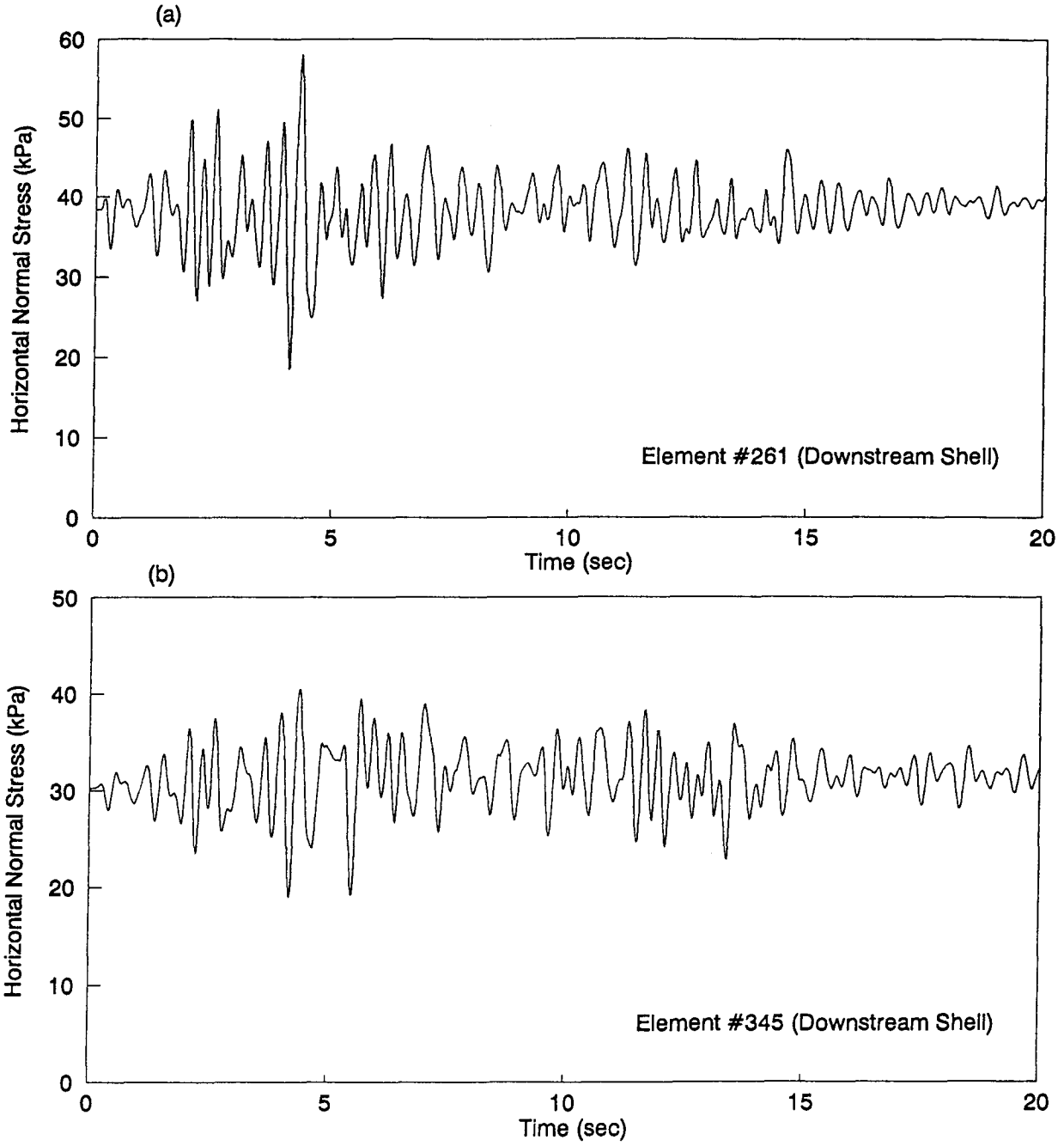

Fig. 5.13 - Horizontal stresses in elements #261 and #345 in Dashihe Dam (1990) (Tangshan Earthquake, 1976)

Chapter 6

POST-LIQUEFACTION ANALYSIS OF DASHIHE DAM (1990)

6.1 Analysis of Post-earthquake Behavior of Dams: Theory and Practice

An important step in the analysis of the seismic stability of dams with potentially liquefiable materials is the determination of whether a flow type of failure involving very large deformations will occur after liquefaction. Liquefaction in this context refers to the loss in shear resistance of soil when subjected to undrained monotonic or cyclic loading. When the soil is loaded undrained beyond its peak strength, the soil may loose a significant amount of its strength and achieve a residual condition at which further shearing would cause no additional change in strength or volume or pore pressure (Seed and Harder, 1990). The shear strength at this point is called the undrained steady state strength or residual strength as shown by curve 1 in Fig. 6.1. If the driving stresses due to gravity on a potential slip surface through liquefied materials in a dam exceeds the residual strength, deformations or sliding of materials will occur until equilibrium is achieved. The more the driving stresses exceed the residual strength, the larger the deformations will occur to achieve a stable condition.

If the strength rises after reaching a minimum value, the phenomenon is called limited liquefaction and is shown by curve 2 in Fig. 6.1. Limited liquefaction may also cause significant deformations due to the strains necessary to develop the strength to restore stability (Finn, 1990).

The conventional limit equilibrium analysis is widely used to evaluate the post-liquefaction stability of an earth dam or foundation. In this method, the factors of safety

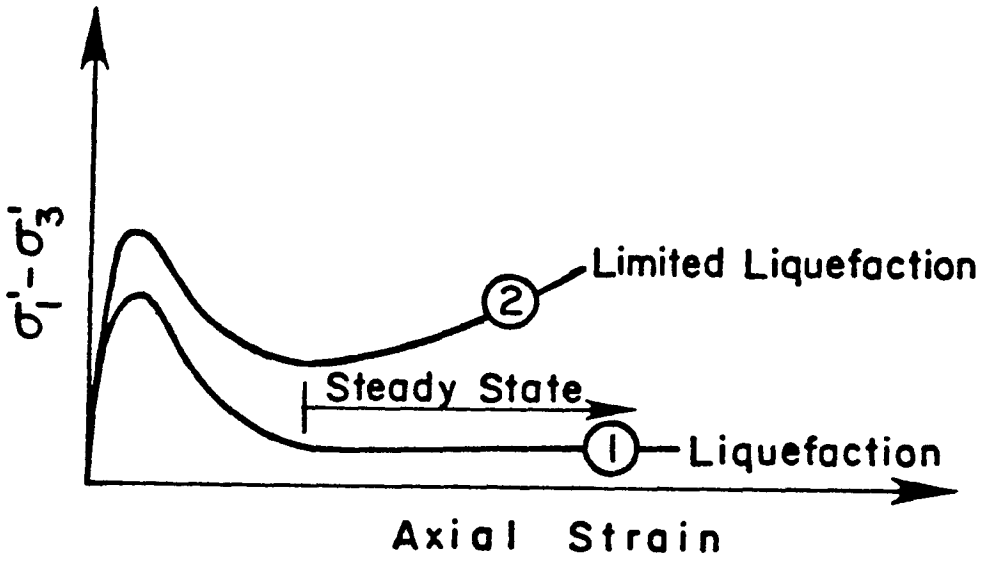

Fig. 6.1 - Types of contractive deformation
(After Vaid et al., 1989; Finn, 1990)

along all potential failure surfaces in the original configuration of the dam are computed taking into account the post-earthquake strengths of all soils. Residual strengths are assigned for liquefied soils. For other soils, the pre-earthquake strengths are reduced to account for the effects of seismic porewater pressures in sands and of cyclic loading in clays. Remedial measures are usually required if the factor of safety drops below some acceptable value. Even if the calculated post-earthquake factors of safety are acceptable, the deformations of the dam should be checked to see if they are within tolerable limits. Deformations may be tolerable even in cases where the factors of safety are less than unity for the undeformed section.

In current practice, if the soil mass does not suffer significant loss in shear strength, deformations are usually estimated using the sliding-block analysis pioneered by Newmark (1965) and modified by Makdisi and Seed (1978). In this method, a potential slip surface in the dam is, first, analyzed statically to determine the inertia force $F_I = (W/g)\, a_y$ that will cause failure, where W is the weight of the sliding block and g is the acceleration due to gravity. The yield acceleration a_y is then deduced from this force. A dynamic analysis of the dam using equivalent linear analysis program such as QUAD-4 (Idriss et al., 1973) is then conducted to determine the average acceleration time history of the sliding mass. The yield acceleration is deducted from the average acceleration time history and the net acceleration is integrated in time twice to obtain the required permanent displacements.

If significant strength loss due to high porewater pressures occurs, then the deformations may be estimated from the shear stress output from dynamic analysis with the aid of laboratory test data (Seed, 1979). The shear stress history in each finite element is,

first, converted to an equivalent number of uniform stress cycles. The strain potential is then determined as that strain developed in a soil element in a cyclic triaxial test under the same initial effective stress conditions as the corresponding element in the field and subjected to the same number of uniform stress cycles. These strains provide an indication of probable seismic deformations in the dam during an earthquake.

An alternative method for computing post-liquefaction deformations was developed by Finn and Yogendrakumar (1989) using a nonlinear finite element program TARA-3FL which is a specialized derivative of TARA-3 program. In this method, the dam is, first, analyzed using pre-earthquake soil strengths and moduli to determine the stress-strain field prior to seismic load application. Seismic loading causes porewater pressures to build-up in saturated cohesionless soils resulting in reduction of the intergranular stresses or effective stresses leading to liquefaction. It is assumed that the residual strengths will be triggered in all soil elements that will liquefy according to the criteria developed by Seed et al. (1985) as is usual in current practice. This process is accompanied by progressive reductions in shear strengths and shear moduli which cause unbalanced shear stresses. The resulting unbalanced stresses in the liquefied elements are redistributed throughout the dam. This sequential and iterative process of strength reduction and stress redistribution is implemented through a series of static finite element analyses. In each step of the deformation analysis, the previous strengths are reduced by a small percentage such as 5 % to simulate a progressive flow deformation of the dam. The final deformed configuration is achieved when the post-earthquake strengths of the soil mass are reached. Since the deformation may become large, it is necessary to update progressively the finite element mesh. Each

calculation of incremental deformation is based on the current shape of the dam, not the initial undeformed shape as in a conventional finite element analysis.

The nonlinear stress-strain behavior of the soil is modelled by an incremental elastic approach using the tangent shear and bulk moduli similar to that implemented in TARA-3. The TARA-3FL procedure has been applied to more than 10 dams since 1989. A typical example is the analysis of the post-liquefaction deformations of Sardis Dam (Finn, 1990).

6.2 Flow Deformation Analysis of Dashihe Dam

The program TARA-3FL described above was used to analyze the flow deformation behavior of the 1990 section of Dashihe Tailings Dam resulting from the effects of seismic excitation anticipated in the field. The results of dynamic analyses previously performed for both the Tangshan and Luanxian earthquakes were used to identify the elements of the dam where liquefaction was triggered and those elements which developed porewater pressures. In the liquefied areas, the shear strengths were assumed to drop to the residual or steady state strength, S_{ur}. These strengths were obtained using the lower bound of the correlation between the residual strength and the normalized standard penetration resistance $(N_1)_{60}$ (Seed and Harder, 1990).

In general design practice, when average $(N_1)_{60}$ values have been chosen to characterize the strengths, stiffness and liquefaction resistance of each material type, it is usual to adopt the lower bound values for the residual strength. In other zones, the seismic porewater pressures derived from the results of dynamic analysis were taken into account in the evaluation of shearing resistance by reducing the friction angle according to the following

equation:

$$\tan \phi_r = (1 - r_u) \tan \phi \qquad (6.1)$$

where ϕ_r is the reduced post-earthquake internal friction angle, ϕ is the pre-earthquake internal friction angle, and r_u is the excess porewater pressure generated by the earthquake normalized by the initial effective overburden pressure. The strength and stiffness parameters of liquefiable materials used in the analysis are presented in Table 6.1. In general, conservative values of the parameters were selected for the analysis.

The predicted final deformed shapes of the dam are shown in Fig. 6.2. It is clear that the Tangshan earthquake would deform the dam more extensively than the Luanxian earthquake due to the fact that the Tangshan earthquake generated more liquefied elements in the dam (see Fig. 5.3). There are no significant displacements in the region of the dam surrounding the crest and the downstream slope. Most of the permanent deformations which occurred were caused by the sliding of materials along the steeper segment of the slope under the pond. Consequently, this could remove support from the beach area and cause extensive cracking in the beach.

The computed vertical and horizontal surface displacements after liquefaction at selected locations throughout the dam are shown in Fig. 6.3. The Tangshan earthquake caused horizontal displacements ranging from 2 m to 13.5 m under the pond. The final deformed shape resembles a large crater that has formed near the edge of the pond as a result of sliding of materials. The vertical displacements reached up to 1.2 m. The pattern of deformations computed for the 1990 section are consistent with the description of earthquake damage observed on the beach near the pond of the 1976 section. From the crack

Table 6.1 - Strength and stiffness parameters used in the post-liquefaction flow deformation analysis of Dashihe Dam (1990)

Zone #	ϕ_r (deg)	S_{ur} (kPa)	$K_{2,max}$	K_b
4	30.9		26.7	4828
5	19.4		26.7	4828
6	32.2		26.7	4828
7	33.6		32.8	5931
8	36.3		36.7	6637
9	34.6		38.8	7016
10	34.6		38.8	7016
11	34.6		38.8	7016
12	37.9		40.8	7378
13	37.8		40.8	7378
14	34.7		38.8	7016
15	34.7		38.8	7016
16	34.7		38.8	7016
17	38.5		42.5	7685
18	34.5		36.7	6637
19	34.5		36.7	6637
20	37.1		35.5	6420
21	33.7		32.8	5931
22	27.1		28.4	5136
23	13.7	5.0	25.0	4521
24	9.1	5.0	25.0	4521

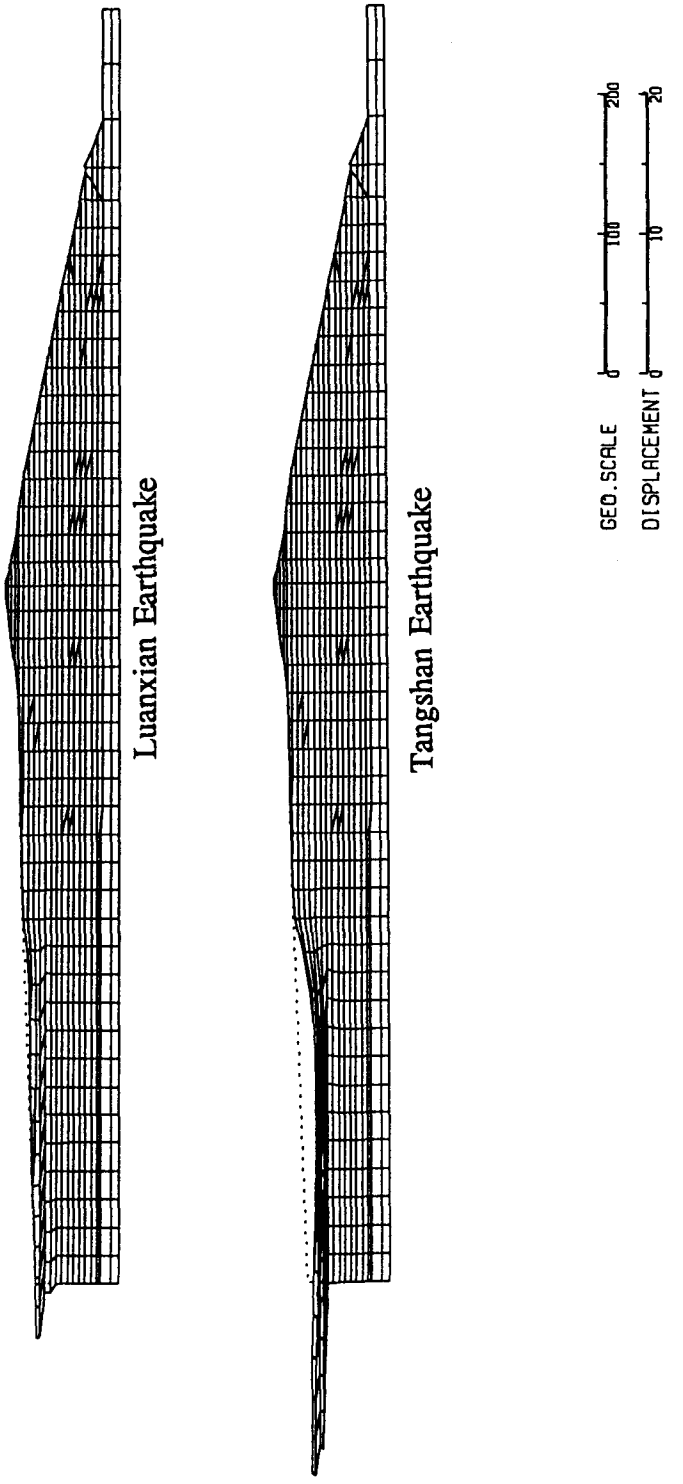

Fig. 6.2 - Computed post-liquefaction deformed shapes of the 1990 Dashihe Dam

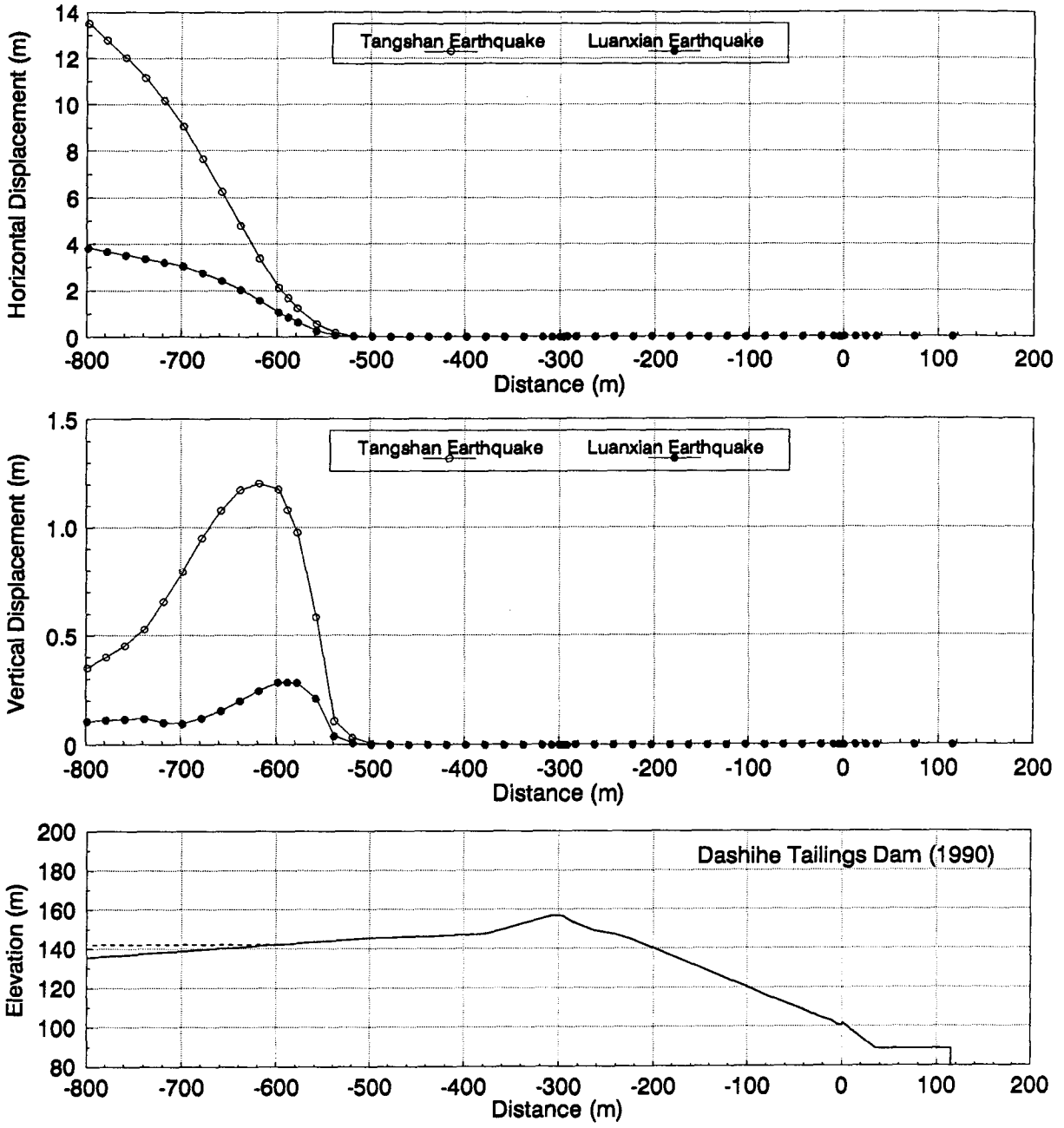

Fig. 6.3 - Computed horizontal and vertical surface displacements induced by liquefaction in Dashihe Dam (1990)

pattern, it was inferred that there had been some significant sliding of materials from the beach towards the pond (Finn and Xin, 1992). The vertical displacements are of the same order of magnitude as those measured at the Xinshui Tailings Dam (1976) around the pond during the 1976 earthquake (CRIBC, 1989). The Xinshui Tailings Dam and Dashihe Tailings Dam were constructed in the same way using similar materials; thus, it is not surprising that their post-liquefaction behavior would be similar when shaken by the same earthquake.

Despite the likely occurrence of significant sliding of beach materials near the pond, the level and extent of damage expected is not likely to impair the ability of the dam to operate. The long and well-designed beach of Dashihe Dam appears capable of adjusting to the expected post-liquefaction deformations in the event of an earthquake similar to the 1976 Tangshan Earthquake.

6.3 Pseudo-static Analysis of Dashihe Dam

Pseudo-static analyses of the stability of both the upstream slope (or beach area) and the downstream slope of the dam before, during and after the earthquake were performed using the XSTABL program (Sharma, 1990). The XSTABL program can automatically generate potential circular failure surfaces and calculate the corresponding factors of safety using the modified Bishop method. Alternatively, non-circular failure surfaces can be analyzed using the Janbu method of slices. Such surfaces are defined by a series of x and y coordinate points connected by straight line segments.

The results of the dynamic analyses were utilized to identify the soil elements that liquefied and to determine the amount of porewater pressure development in other elements

that did not liquefy. Residual strengths were assigned to liquefied soils and for others pre-earthquake strengths were reduced to account for the effects of seismic porewater pressures as discussed in the previous section.

The results of the dynamic analyses indicate that, in most cases, triggering of liquefaction occurred during the early stage of shaking. Also, in other elements, porewater pressures reached maximum values a few seconds before the shaking stopped. Therefore, it is appropriate to take into account in the analysis the effects of seismic loading on the stability of the dam by applying pseudo-static forces on the potential sliding mass.

The most critical failure surfaces in both the downstream and upstream slopes corresponding to seismic coefficient, k = 0 were initially determined. Then, the distribution of peak response accelerations in the potential sliding masses were obtained from the results of the dynamic analyses. Figure 6.4 shows the statistical frequency distribution of peak accelerations at node points inside the potential sliding masses obtained from dynamic analyses output. The peak response accelerations in the upstream slope ranged from 0.05 to 0.15 g with an average value of 0.10 g, while in the downstream slope they ranged from 0.08 to 0.24 g, with an average value of 0.13 g. These average accelerations are used later in the interpretation of dam behavior from the results of pseudo-static analyses that used a wide range of values of seismic coefficient k.

Figure 6.5 shows the computed factors of safety, Fs, of the critical failure surfaces in the 1990 Dashihe Dam for different values of k, i.e., from 0 to 0.15 for the upstream slope, and 0 to 0.24 for the downstream slope.

Before the earthquake, the minimum factor of safety of the upstream slope was high

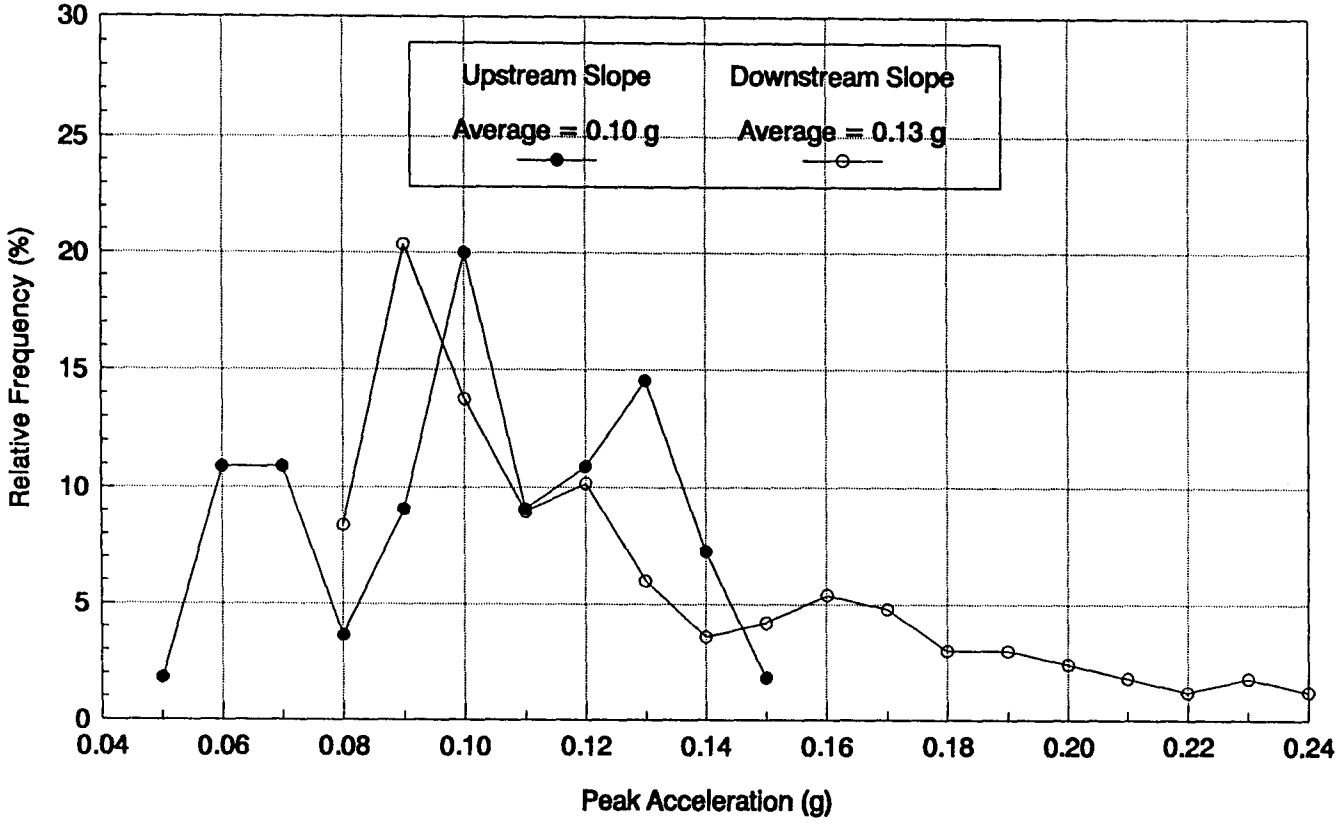

Fig. 6.4 - Frequency distribution of peak nodal accelerations inside the potential sliding masses (Tangshan Earthquake, 1976)

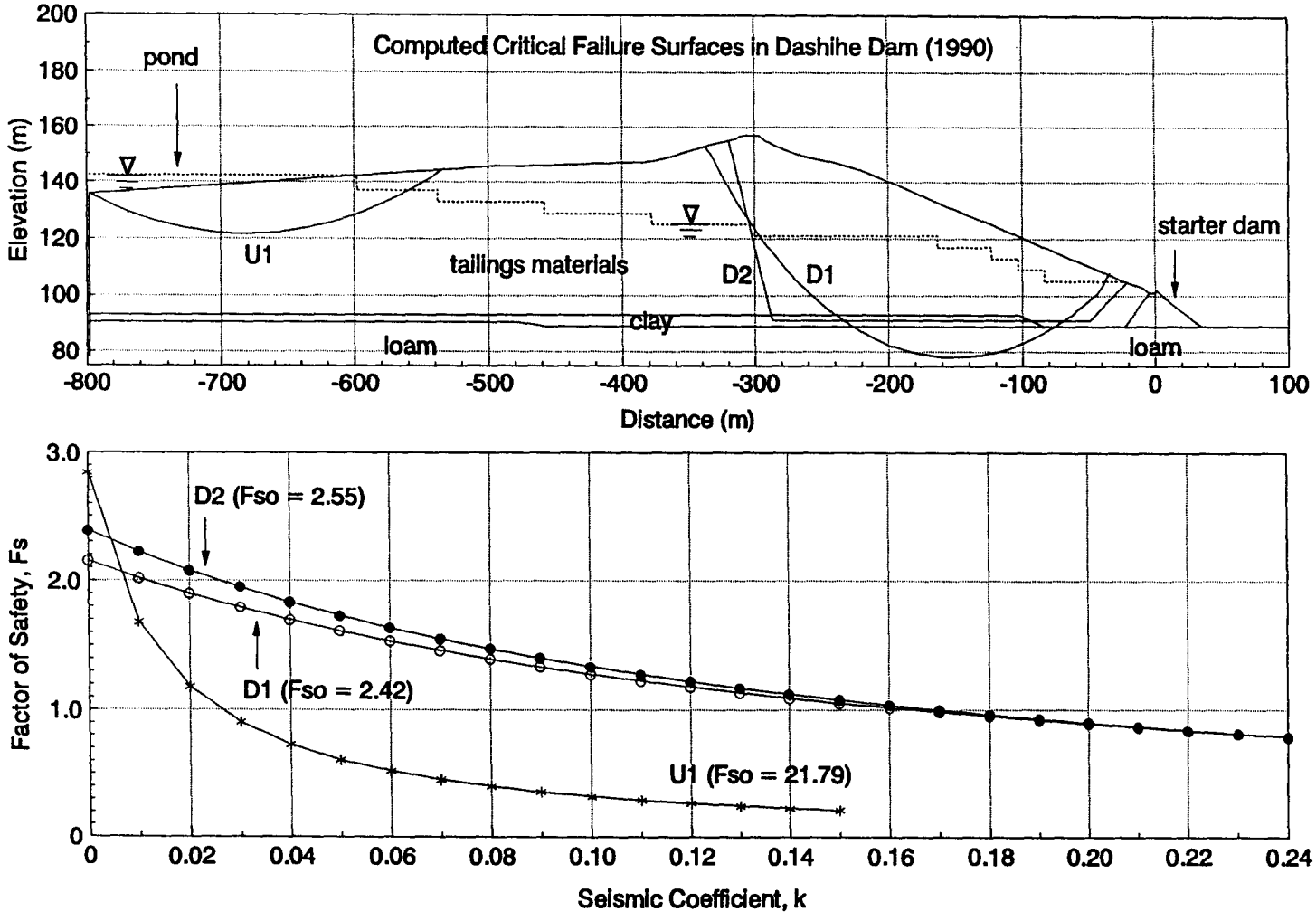

Fig. 6.5 - Results of pseudo-static stability analysis of the 1990 Dashihe Dam (Tangshan Earthquake, 1976)

(Fso = 21.79). However, the earthquake-induced liquefaction and high porewater pressures which developed under the beach near the pond greatly reduced the stability of the upstream slope. The critical value of seismic coefficient or the value of k which gives a factor of safety of unity is about 0.03. Since the expected level of acceleration of the sliding mass in the upstream slope is much larger than 0.03 g, sliding of the upstream slope materials toward the pond as indicated by surface U1 is predicted to occur. It is interesting to notice that the general shape and location of the most critical failure surface determined from pseudo-static analysis is compatible with the computed pattern of flow deformation of the upstream slope.

Greater confidence is required in the stability analysis of the downstream slope because the consequences of a failure in this area of the dam would be catastrophic due to large amount of materials that would be displaced. Therefore, both circular and non-circular potential failure surfaces in the downstream slope were analyzed. In particular, the non-circular failure surfaces were made to pass through the thin clay layer at the base of the dam with undrained strength, Su = 164 kPa overlying the stiff loam foundation of the dam with Su = 312 kPa (Fig. 6.5). In the analysis presented in Fig. 6.5, the possible reduction in the strength of the clay layer due to cyclic loading is initially ignored due to lack of data. The results show that the most critical failure surface, D1, had a factor of safety of 2.42 before the earthquake. After the earthquake, a factor of safety of unity would be achieved when the average acceleration of the potential sliding mass in the downstream slope becomes equal to 0.17 g. However, dynamic analysis output shows that the expected average acceleration of the potential sliding mass in the downstream slope is only 0.13 g. Therefore, such failure of the downstream slope is unlikely to occur. In addition, previous flow deformation analysis

results show that no significant displacement is predicted to occur in the downstream slope.

Since the critical failure surfaces in the downstream slope pass through a significant portion of the foundation materials, it is important to investigate the effect of strength reduction in the thin clay layer on the stability of the dam. However, no laboratory data is available for evaluating the exact amount of strength reduction in the clay layer; thus, it is not possible to determine the proper combination of seismic coefficient and strength reduction that should be used in the seismic stability analysis of the dam. Based on previous laboratory tests on undisturbed and remolded samples of different clayey materials (Thiers and Seed, 1968), Makdisi and Seed (1978) have shown that, in most cases, the cyclic yield strength of a clay can be taken to be about 80 % or more of the static undrained strength. Therefore, all potential failure surfaces passing through the clay layer were analyzed for different combination of seismic coefficients and reductions of 5 to 20 % in the strength of the clay layer. The location of the most critical failure surface, D2, is shown in Fig. 6.5. The computed factors of safety for failure surface D2 are given in Table 6.2. The factor of safety decreases when either the seismic coefficient or the amount of strength reduction in the clay layer is increased. Assuming that the acceleration of the potential sliding mass in the downstream slope is about 0.13 g, the factor of safety of the downstream slope would range from 1.02 to 1.13 depending on the amount of strength reduction in the clay layer at the base of the dam. Therefore, the downstream slope in the 1990 configuration of Dashihe Dam would remain stable when shaken by a ground motion equivalent to the 1976 Tangshan Earthquake even if some strength reductions in the clay layer is considered.

Table 6.2 - Computed factors of safety for different combination of seismic coefficients and strength reductions in the thin clay layer due to earthquake loading (1990 Dashihe Dam - Downstream Slope)

Seismic Coefficient k (g)	Factor of Safety, Fs			
	5 % Strength Reduction	10 % Strength Reduction	15 % Strength Reduction	20 % Strength Reduction
0.10	1.30	1.25	1.21	1.17
0.11	1.24	1.19	1.16	1.12
0.12	1.18	1.14	1.11	1.07
0.13	1.13	1.09	1.06	1.02
0.14	1.09	1.05	1.02	0.98
0.15	1.04	1.01	0.98	0.94
0.16	1.00	0.97	0.94	0.90
0.17	0.97	0.94	0.90	0.87

Chapter 7

SUMMARY AND CONCLUSIONS

The seismic response of the Dashihe Tailings Dam in its 1990 condition was investigated using the nonlinear dynamic effective stress analysis program TARA-3 (Finn et al., 1986). Zones of liquefaction under the pond and the beach are predicted to develop in the dam if it is shaken by an earthquake equivalent to the 1976 Tangshan Earthquake. Extensive cracking is predicted to occur in the beach over a distance of 160 m from the pond margin in the direction of the crest of the dam. Input accelerations were amplified in the region of the dam surrounding the crest and the downstream slope where minimal values of porewater pressures were generated. On the other hand, substantial deamplification of motions occurred under the pond and the beach where liquefaction and high porewater pressures developed. These results show the dependence of seismic response on the level of seismic porewater pressures.

Potential post-liquefaction flow deformations of the dam were computed using the program TARA-3FL (Finn and Yogendrakumar, 1989). The results show that no significant displacements would occur in the downstream slope or around the crest of the dam because of the low seismic porewater pressures which developed in these areas. Most of the deformations are predicted to occur by sliding of materials under the pond and a significant portion of the beach close to the pond margin. The analysis also shows that the Tangshan earthquake was more effective in causing large permanent deformations than the Luanxian earthquake because the Tangshan earthquake generated more liquefied elements in the dam.

Horizontal displacements ranging from 2 to 13.5 meters and vertical diplacements of up to 1.2 meters are predicted to occur under the pond. However, these deformations are not likely to impair the ability of the dam to operate.

Pseudo-static analyses of the stability of both the upstream slope (or beach area) and the downstream slope of the dam before, during and after the earthquake were also performed using the program XSTABL (Sharma, 1990). The factors of safety along all potential failure surfaces in the undeformed configuration of the dam are computed taking into account the reduction in strengths of all soils. Residual strengths are assigned for liquefied soils. For other soils, the original static strengths are reduced to account for the effects of seismic porewater pressures in sands and of cyclic loading in clays. Pseudo-static forces are applied on the potential sliding masses to take into account the effects of seismic loading on the stability of the dam. The potential failure surfaces in the dam are analyzed for different values of seismic coefficient, i.e., from 0 to 0.15 for the upstream slope, and from 0 to 0.24 for the downstream slope. Based on the results of the dynamic analyses, the average peak accelerations of the potential sliding masses in the upstream and downstream slopes are 0.10 g and 0.13 g, respectively. Potential instability of the materials under the pond and a significant portion of the beach in the upstream slope is predicted to occur due to the development of liquefaction and high seismic porewater pressures in these areas. The factor of safety of the upstream slope is reduced from 21.79 before the earthquake to less than unity when $k = 0.10$, corresponding to the expected average acceleration of the sliding mass. On the other hand, the downstream slope is predicted to remain stable after the earthquake. When $k = 0.13$, corresponding to the expected average acceleration of the

sliding mass in the downstream slope, the factor of safety ranges from 1.02 to 1.13 for 20 to 5 % reductions in the strength of the clay layer at the base of the dam.

The analysis presented in this thesis represents a research study of the seismic response and post-liquefaction behavior of the Dashihe Tailings Dam in its 1990 configuration to the specified shaking from the Tangshan and Luanxian earthquakes. The sensitivity studies that are an essential part of making decisions regarding the safety of the dam in its 1990 condition have not been made. The use of Tangshan and Luanxian input motions in the analysis of the 1976 and 1990 configurations does not imply that these motions are appropriate motions for making a seismic safety evaluation of the Dashihe Dam in its present or any future configuration. Therefore, no inference should be drawn about the safety of raising the dam above the 1990 configuration from the results of this study.

BIBLIOGRAPHY

Aki, K. (1988). *Local Site Effects on Strong Ground Motion.* in J.L. Van Thun (ed.), "Earthquake Eng. and Soil Dynamics: Recent Advances in Ground Motion Evaluation," ASCE Geotech. Special Publication No. 20, 103-155.

Byrne, P.M. (1991). *A Cyclic Shear-Volume Coupling and Pore Pressure Model for Sand.* Proc., 2nd Int. Conf. on Recent Advances in Geotech. Earthquake Eng. & Soil Dynamics, St. Louis, Missouri, U.S.A., March 11-15, 47-56.

Castro, G., Keller, T.O. and Boynton, S.S. (1989). *Re-evaluation of the Lower San Fernando Dam.* Report No. 1, GL-89-2, U.S. Army Corps of Engineers, Waterways Experiment Station, Vicksburg, Mississippi, U.S.A.

Celebi, M. and Hanks, T. (1986). *Unique Site Response Conditions of Two Major Earthquakes of 1985: Chile and Mexico.* Proc. of the Int. Symposium of Eng. Geology Problems in Seismic Areas, Bari, Italy.

CIGHS (1980). *Field Investigation on Dashihe Tailings Dam* (in Chinese). A Report by the Central Institute of Geotechnics, Geophysics, Hydrogeology and Surveying, Ministry of Mineral Industries, Biaoding, China.

CRIBC (1989). *Characteristics of Tangshan Earthquake and Determination of Seismic Parameters in Dashihe Tailings Dam Site.* A Report by the Central Research Institute of Building and Construction, Beijing, China.

CRIBC (1990). *Field Investigation on Dashihe Tailings Dam.* A Report by the Central Research Institute of Building Construction, Beijing, China.

CRIBC (1991). *Laboratory Test Report for Reconstituted Samples.* Report 3-3-1 for the Sino-Canadian Joint Investigation on Earthquake Safety of Chinese Tailings Dams.

Duncan, J.M., Byrne, P.M., Wong, K.S., and Mabry, P. (1978). *Strength, Stress-Strain and Bulk Modulus Parameters for Finite Element Analyses of Stresses and Movements in Soil Masses.* Report No. WCB/GT/78-02 to the National Science Foundation.

Faccioli, E. (1991). *Seismic Amplification in the Presence of Geological and Topographic Irregularities.* Proc. of the 2nd Int. Conf. on Recent Advances in Geotech. Earthquake Eng. and Soil Dynamics, St. Louis, Missouri, U.S.A., 1779-1797.

Finn, W.D. Liam (1988). *Dynamic Analysis in Geotechnical Engineering.* State-of-the-art Lecture, Proc. of the ASCE Conf. on Earthquake Eng. and Soil Dynamics, Park City, Utah, U.S.A.

Finn, W.D. Liam (1990). *Analysis of Post-liquefaction Deformations in Soil Structures.* Proc. of H.Bolton Seed Memorial Symposium, Vol. 2 (Ed. M. Duncan), Bi-Tech Publishers.

Finn, W.D. Liam (1991). *Assessment of Liquefaction Potential and Post-liquefaction Behavior of Earth Structures: Developments 1981-1991.* State-of-the-art Paper, Proc. of the 2nd Int. Conf. on Recent Advances in Geotech. Earthquake Eng. and Soil Dynamics, St.Louis, Missouri, U.S.A., March 11-15, 1833-1850.

Finn, W.D. Liam, Lo, R.C. and Yogendrakumar, M. (1987). *Dynamic Nonlinear Analysis of Lukwi Tailings Dam.* A Report by the Soil Dynamics Group, Dept. of Civil Eng., Univ. of British Columbia, Vancouver, Canada.

Finn, W.D. Liam and Xin, H.B. (1992). *Seismic Response and Stability Analysis of the 1976 Dashihe Tailings Dam.* A Report for the Sino-Canadian Joint Investigation on Earthquake Safety of Chinese Tailings Dams.

Finn, W.D. Liam, Xin, H.B. and Wang, Y.Q. (1992). *Lessons from Seismic Performances of Chinese Tailings Dams.* Report, Dept. of Civil Eng., Univ. of British Columbia, Vancouver, Canada.

Finn, W.D. Liam, Yogendrakumar, M., Yoshida, N. and Yoshida, H. (1986). *TARA-3: A Program to Compute the Response of 2-D Embankments and Soil Structure Interaction Systems to Seismic Loadings.* Dept. of Civil Eng., Univ. of British Columbia, Vancouver, Canada.

Gao, J.S., Robertson, P.K. and Morgenstern, N.R. (1991). *Site Data Analysis on Dashihe Tailings Dam.* Report 3-2-1 for the Sino-Canadian Joint Investiagation on Earthquake Safety of Chinese Tailings Dams.

Hu, Y. et al. (1986). *Attenuation Relationship of Ground Motion from North China Partly Based on Data from Tangshan Earthquake.* Chinese Journal of Civil Engineering.

Idriss, I.M., Lysmer, J., Hwang, R. and Seed, H.B. (1973). *QUAD-4: A Computer Program for Evaluating the Seismic Response of Soil Structures by Variable Damping Finite Element Procedures.* Report No. EERC 73-16, Earthquake Eng. Research Center, Univ. of California, Berkeley, California, U.S.A.

Li, W.S., Robertson, P.K. and Morgenstern, N.R. (1992). *Laboratory Test Data Analysis on Dashihe Tailings Sands.* Report 3-5 for the Sino-Canadian Joint Investigation on Earthquake Safety of Chinese Tailings Dams.

Lo, R.C. and Klohn, E.J. (1990). *Seismic Stability of Tailings Dams.* Proc. of the Int. Symposium on Safety and Rehabilitation of Tailings Dams, Int. Commission on Large Dams, Sydney, Australia, Vol. 1, 90-105.

Makdisi, F.I. and Seed, H.B. (1978). *A Simplified Procedure for Estimating Dam and Embankment Earthquake-Induced Deformations*. J. of the Geotech. Eng. Div., ASCE, Vol. 104, No. GT7, 849-867.

Marcuson, W.F. III, Hynes, M.E. and Franklin, A.G. (1990). *Evaluation and Use of Residual Strength in Seismic Safety*. Earthquake Spectra, Vol. 6, No. 3, 529-572.

Martin, G.R., Finn, W.D. Liam and Seed, H.B. (1976). *Fundamentals of Liquefaction Under Cyclic Loading*. J. of the Geotech. Eng. Div., ASCE, Vol. 101, GT5, 324-438.

Newmark, N.M. (1965). *Effects of Earthquake on Dams and Embankments*. 5th Rankine Lecture, Geotechnique 15, No. 2, 139-160.

Poulos, S.J., Castro, G. and France, J.W. (1985). *Liquefaction Evaluation Procedure*. J. of the Geotech. Eng. Div., ASCE, Vol. 111, No. GT6, 772-795.

PWRI (1986). *Dense Instrument Array Observation of Strong Earthquake Motion*. A Report by the Public Works Research Institute, Ministry of Construction, Tsukuba, Japan.

Schmertmann, J.H. and Palacios, A. (1979). *Energy Dynamics of SPT*. J. of the Geotech. Eng. Div., ASCE, 909-1045.

Scott, M.D., Lo, R.C., Klohn, E.J., Finn, W.D.L. and Yogendrakumar, M. (1989). *Nonlinear Dynamic Analysis of L-L Tailings Dam*. Proc. of the 12th Conf. of Int. Society of Soil Mech. and Found. Eng., Rio de Janeiro, Brazil, Vol. 3, 1911-1914.

Seed, H.B. (1979). *Considerations in the Earthquake-Resistant Design of Earth and Rockfill Dams*. 19th Rankine Lecture, Geotechnique 29, No. 3, 215-263.

Seed, H.B. (1987). *Design Problems in Soil Liquefaction*. J. of the Geotech. Eng. Div., ASCE, Vol. 113, No. GT7, 827-845.

Seed, H.B. and Idriss, I.M. (1970). *Soil Moduli and Damping Factors for Dynamic Response Analyses*. Report No. EERC-70-10, Earthquake Eng. Research Center, Univ. of California, Berkeley, California, U.S.A.

Seed, H.B., Seed, R.B., Harder, L.F. and Jong, H.L. (1988). *Re-evaluation of the Slide in the Lower San Fernando Dam in the Earthquake of Feb. 9, 1971*. Report No. EERC 88-4, Earthquake Eng. Research Center, Univ. of California, Berkeley, California, U.S.A.

Seed, H.B., Tokimatsu, K., Harder, L.F. and Chung, R.N. (1984). *The Influence of SPT Procedures in Soil Liquefaction Resistance Evaluations*. Report No. EERC 84-15, Earthquake Eng. Research Center, Univ. of California, Berkeley, California, U.S.A.

Seed, H.B., Wong, R.T., Idriss, I.M. and Tokimatsu, K. (1986). *Moduli and Damping Factors for Dynamic Analyses of Cohesionless Soils*. J. of the Geotech. Eng. Div., ASCE, Vol. 112, No. GT11, 1016-1032.

Seed, R.B. and Harder, L.F. (1990). *SPT-Based Analysis of Pore Pressure Generation and Undrained Residual Strength*. Proc. of the H.B. Seed Memorial Symposium, J.M. Duncan (Ed.), Vol. 2, 351-376.

Sharma, S. (1990). *XSTABL: An Integrated Slope Stability Analysis Program for Personal Computers*. Interactive Software Designs, Inc.

Thiers, G. and Seed, H.B. (1968). *Cyclic Stress-Strain Characteristics of Clay*. J. of the Soil Mechanics and Foundation Div., ASCE, Vol. 94, No. SM2, 555-569.

Vaid, Y.P. and Chern, J.C. (1985). *Cyclic and Monotonic Undrained Response of Saturated Sands*. Proc. of ASCE National Convention, Session- Advances in the Art of Testing Soils Under Cyclic Loading, Detroit, 120-147.

Vaid, Y.P., Chung, E.K.F., and Kuerbis, R.H. (1989). *Stress Path and Steady State*. Canadian Geotech. Journal, Vol. 27, No. 1.

Yogendrakumar, M. and Finn, W.D. Liam (1986). *SIMCYC2: A Program for Simulating Cyclic Simple Shear Tests on Dry or Saturated Sands*. Report by the Soil Dynamics Group, Dept. of Civil Eng., Univ. of British Columbia, Vancouver, Canada.

Appendix I

DESCRIPTION OF TARA-3 PROGRAM

Method of Analysis

An incremental approach is used to estimate the nonlinear behavior of soil using tangent and shear moduli, G_t and B_t respectively. The equations of dynamic equilibrium are given by:

$$[M]\{\Delta \ddot{x}\} + [C]\{\Delta \dot{x}\} + [K]\{\Delta x\} = \{\Delta P\} \qquad \text{(A-I.1)}$$

where *[M]*, *[C]* and *[K]* are the mass, damping and stiffness matrices respectively; $\{\Delta \ddot{x}\}$, $\{\Delta \dot{x}\}$ and $\{\Delta x\}$ are the matrices of incremental relative accelerations, velocities and displacements; and $\{\Delta P\}$ are the incremental dynamic forces. The viscous damping is of the Rayleigh type and its use is optional. Very small amounts of viscous damping are used to control any high frequency oscillations that may arise from numerical integration. Damping is mainly hysteretic and is automatically included as the hysteretic stress-strain loops are executed during analysis.

Nonlinear Stress-Strain Behavior

The soil behavior is assumed to be nonlinear and hysteretic and follows Masing behavior during unloading and reloading. Masing behavior provides hysteretic damping.

The relationship between shear stress and shear strain for the initial loading phase under drained or undrained conditions is assumed to be hyperbolic. The tangent shear

modulus, G_t, for a point on the initial loading curve is given by:

$$G_t = \frac{G_{max}}{\left(1 + \frac{G_{max}\,|\gamma|}{\tau_{max}}\right)^2} \qquad \text{(A-I.2)}$$

in which G_{max} is the maximum shear modulus, τ_{max} is the appropriate shear strength of the soil and γ is the induced shear strain. At a stress point on an unloading or reloading curve G_t is given by:

$$G_t = \frac{G_{max}}{\left(1 + \frac{G_{max}}{2\,\tau_{max}}\,|\gamma - \gamma_r|\right)^2} \qquad \text{(A-I.3)}$$

The maximum shear modulus for sands is computed by:

$$G_{max} = 21.7\ P_a\ K_{2,max} \left(\frac{\sigma'_m}{P_a}\right)^{1/2} \qquad \text{(A-I.4)}$$

where P_a is the atmospheric pressure, σ_m is the mean effective stress, and $K_{2,max}$ is a parameter that depends on material type and density. A site-specific relationship between $K_{2,max}$ and the normalized SPT blowcount $(N_1)_{60}$ has been established in Chapter 4 (shown in Fig. 4.8) based on shear wave velocity measurements in the field.

For clayey soils, G_{max} is evaluated by the following expression:

$$G_{max} = K_c\ S_u \qquad \text{(A-I.5)}$$

in which K_c is the undrained shear modulus constant for a given clay, and S_u is the undrained shear strength of the clay.

The response of the soil to isotropic compression is assumed to be nonlinearly elastic and a function of the mean normal stress. Neglecting hysteretic behavior in this mode, if any, the relationship between tangent bulk modulus, B_t, and the mean normal effective stress, σ_m is expressed as follows:

$$B_t = K_b P_a \left(\frac{\sigma'_m}{P_a} \right)^n \qquad \text{(A-I.6)}$$

in which K_b is the bulk modulus coefficient and n is the bulk modulus exponent.

Porewater Pressure Generation Model

During seismic shaking, both transient and residual porewater pressures are generated in saturated sands. The transient changes in porewater pressures are equal to the changes in the mean normal stresses. Since they balance each other, the effective stress regime in the sand remains largely unchanged and so the stability and deformability of the sand is not seriously affected. Therefore, these pressures are neglected in TARA-3.

The residual porewater pressures result from plastic deformations in the sand skeleton during seismic loading. These pressures remain until dissipated by drainage or diffusion and therefore they exert a major influence on the strength and stiffness of the sand skeleton.

The residual porewater pressures are computed in TARA-3 using the model developed by Martin, Finn and Seed (1975). In this model, the increments in porewater pressure, Δu, that develop in a saturated sand during undrained seismic shear straining are related to the

volumetric strain increments, $\Delta\varepsilon_{vd}$, that occur in the same sand under drained conditions with the same shear strain history. The porewater pressure model is described by:

$$\Delta u = E_r \, \Delta\varepsilon_{vd} \qquad \text{(A-I.7)}$$

in which E_r is the one-dimensional rebound modulus of sand.

Under drained simple shear conditions, the volumetric strain increment $\Delta\varepsilon_{vd}$ is a function of the total accumulated volumetric strain ε_{vd} and the amplitude of the current shear strain γ (Martin, Finn and Seed, 1975). A simplified expression of this relationship proposed by Byrne (1991) is given by:

$$\Delta\varepsilon_{vd} = \gamma \, C_1 \, e^{\frac{-C_2 \, \varepsilon_{vd}}{\gamma}} \qquad \text{(A-I.8)}$$

in which C_1 and C_2 are volume change constants which depend on the material type and relative density and may be determined directly by means of drained cyclic simple shear tests on dry or saturated samples (Martin, Finn and Seed, 1975) or derived from field data as discussed in Chapter 4. In two-dimensional analysis in practice, the permanent volume changes due to shearing action are related to the cyclic shear stresses on horizontal planes because the seismic input motions are usually assumed to be shear waves propagating vertically. Therefore, in TARA-3, for computation of $\Delta\varepsilon_{vd}$ in equation (A-I.8) the shear strain on the horizontal plane, γ_{xy} is substituted in place of γ.

Martin, Finn and Seed (1975) developed an empirical equation for the rebound modulus E_r, at a given stress level σ_v, given by:

$$E_r = \frac{(\sigma'_v)^{1-m}}{m\, K_2\, (\sigma'_{vo})^{n-m}} \qquad \text{(A-I.9)}$$

in which σ_{vo} is the initial value of the effective stress and K_2, m and n are experimental constants derived from rebound tests in a consolidation ring.

In current engineering practice, dynamic analyses are usually conducted without including the effects of gravity or previous strains. In TARA-3, a static analysis is first carried out to determine the initial stress conditions throughout the dam to estimate the initial moduli to be used in the subsequent dynamic analysis. As porewater pressures increase in saturated soils during seismic shaking, the effective stresses decrease. The effective stress system is continually updated by solving the equilibrium equations while taking the increments in porewater pressure into account. The incremental displacements, strains and stresses given by this procedure constitute the response of the structure to softening of the elements. the incremental strains are accumulated and they contribute to the permanent deformations of the soil structure. Both shear and bulk moduli are adjusted to be compatible with the updated effective stress system.